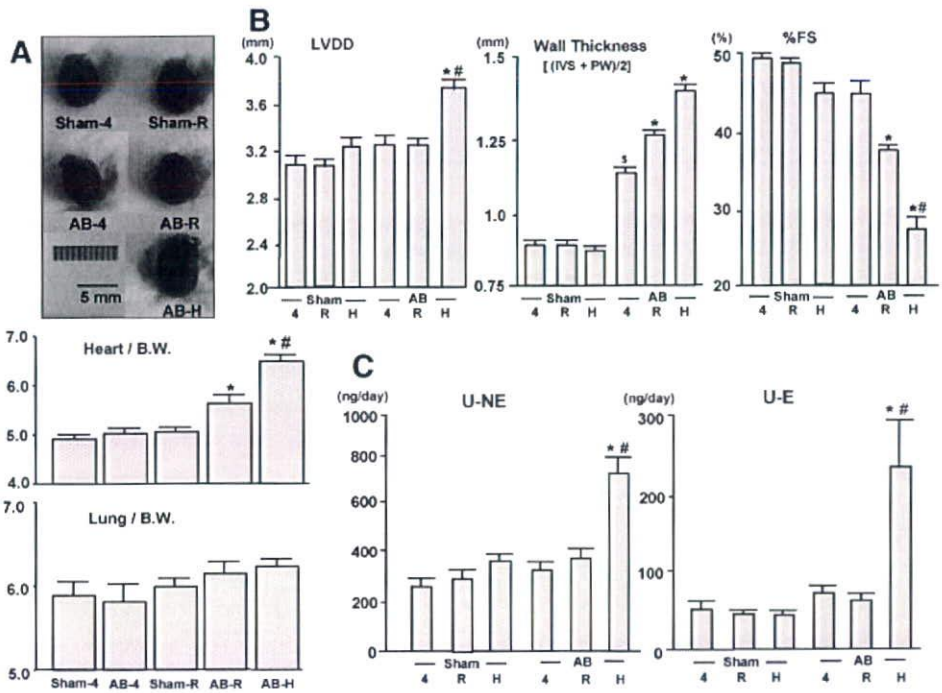

Figure 2. A, Example of the heart in each group and the relative heart and lung weight in each group. *$P<0.05$ vs Sham-4 and Sham-R, #$P<0.05$ vs AB-R (n=6 in each group). B, Cardiac function evaluation by echocardiography in each group. IVS, interventricular septum; PW, posterior wall. *$P<0.05$ vs Sham-R, #$P<0.05$ vs AB-R, \$$P<0.05$ vs Sham-4 (n=8 in each group). C, The 24-hour U-NE and U-E excretion in each group. *$P<0.05$ vs Sham-4 and Sham-R, #$P<0.05$ vs AB-R (n=10 in each group).

formed as described earlier. See the online data supplement for details.

Evaluation of the Effects of Rho-Kinase and Angiotensin Type 1 Receptor Blockade in the Brain

To assess the effects of Rho-kinase or angiotensin II type 1 receptor (AT_1R) blockade in the brain, Y-27632 (a specific Rho-kinase inhibitor[18]) or telmisartan (an AT_1R blocker) was infused ICV (Y-27632: 5 mmol/L, 0.11 μL/h for 28 days; telmisartan: 4 and 20 mmol /L, 0.11 μL/h for 28 days). The U-NE and U-E excretion, arterial pressure, heart rate, and organ weight were measured, and echocardiography was performed as described earlier. See the online data supplement for details.

Evaluation of AT_1R Expression and Rho-Kinase Activity

To assess AT_1R expression levels and Rho-kinase activity, we performed a Western blot analysis for AT_1R (1:1000, Santa Cruz Biotechnology, Santa Cruz, Calif) and phosphorylated-moesin, a substrate of Rho-kinase[19] (p-moesin, 1:1000, Santa Cruz Biotechnology) in the circumventricular tissues, including the hypothalamus and brain stem tissues, of Sham-4 mice and AB-4 mice. See the online data supplement for details.

Statistical Analysis

All values are expressed as means±SE. ANOVA was used to compare U-NE and U-E excretion, organ weight, left ventricular end-diastolic diameter (LVDD), left ventricular wall thickness (LVWT), percentage fractional shortening (%FS), and arterial pressure measured by telemetry between groups. An unpaired *t* test was used to compare changes in arterial pressure and heart rate after high-Na ICV infusion, as well as protein levels, between Sham mice and AB mice. Differences were considered to be significant when $P<0.05$.

Results

Characteristics of the Pressure Overload Model

Relative heart weight (heart weight/body weight) was not increased in AB-4 mice compared with Sham-4 mice (Figure 2A). AB-R mice, however, had a significantly higher relative heart weight than Sham-R mice and a significantly lower relative heart weight than AB-H mice. Relative lung weight (lung weight/body weight) did not differ between groups (Figure 2A). Body weight of AB mice was significantly lower than that of Sham mice (body weight: Sham-4, 44.7±1.4 g; AB-4, 45.3±1.1 g; Sham-R, 47.8±0.5 g; AB-R, 42.5±0.6 g; AB-H 40.6±0.9 g, n=6 for each); however, the absolute heart weight in AB-H was significantly greater than that in AB-R or Sham-R mice (heart weight: AB-H 0.26±0.01 g; Sham-R 0.24±0.01 g; AB-R 0.24±0.01 g; n=6 for each).

Echocardiography revealed the following characteristics: LVWT was greater in AB-4 mice than in Sham-4 mice, but %FS did not differ between the groups (Figure 2B). After an additional 4 weeks, cardiac function declined in AB-R mice compared with Sham-R mice and declined significantly more in AB-H mice compared with AB-R mice. LVDD was also higher in AB-H mice than in AB-R mice (Figure 2B).

Sympathetic activity was not significantly different among the AB-4 mice, AB-R mice, Sham-4 mice, and Sham-R mice. U-NE and U-E excretion was significantly higher, however, in AB-H mice compared with the other groups (Figure 2C).

LVEDP was significantly higher in AB-4 mice than in Sham-4 mice. In addition, LVEDP in AB-H mice further increased compared with Sham-R or AB-R mice (Table I in the online data supplement).

Arterial Pressure Monitoring

Measurement Under Anesthesia

Mean arterial pressure and heart rate were significantly higher in AB-4 mice compared with Sham-4 mice. In AB-R and AB-H mice, arterial pressure was reduced to levels similar to that in the Sham-R mice. Heart rate was significantly higher in AB-4, AB-R, and AB-H mice than in Sham-4

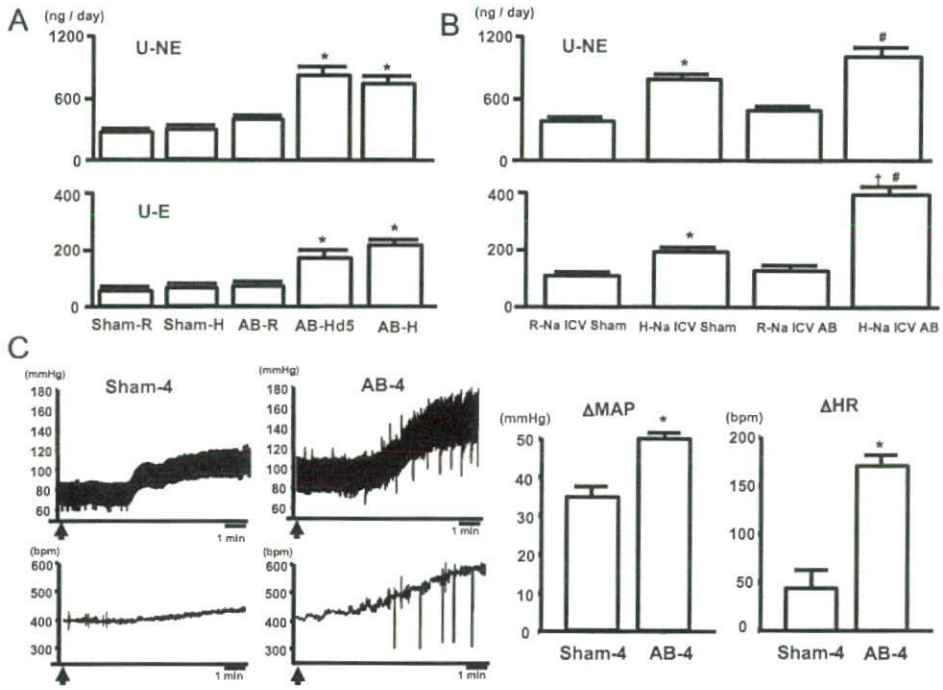

Figure 3. A, The 24-hour U-NE and U-E excretion in each group (response of sympathetic activity to high-salt diets). *$P<0.05$ vs Sham-R, Sham-H, and AB-R (n=10 in each group). B, The 24-hour U-NE and U-E excretion in each group (response of sympathetic activity to high-Na aCSF ICV infusion). *$P<0.05$ vs ICV R-Na Sham, #$P<0.05$ vs ICV R-Na AB, †$P<0.05$ vs high-Na ICV Sham (n=5 in each group). C, Response of arterial pressure and heart rate to ICV high-Na aCSF infusion. Left, Representative recordings from Sham-4 and AB-4 showing arterial pressure and heart rate response to ICV high-Na aCSF infusion. Right, Group data of mean arterial pressure and heart rate response to ICV high-Na aCSF infusion in Sham-4 and AB-4. *$P<0.05$ vs Sham (n=3 in each group).

or Sham-R mice. There were no significant differences in arterial pressure and heart rate between the groups of Sham mice (Online Table II).

Measurement in Awake Mice Using Radio-Telemetry System

In AB-4 mice (AB day 28), mean arterial pressure and heart rate were significantly higher than that in the mice before aortic banding. Furthermore, high salt intake (AB-H mice) dramatically increased mean arterial pressure to 171±5 mm Hg by day 35 after aortic banding (1 week after the starting high salt intake). The general conditions deteriorated in all AB-H mice, however, likely because of severe lung congestion (lung/body weight ratio, 7.0±0.1). In AB-R mice, mean arterial pressure increased mildly, and the highest mean arterial pressure value was 145±5 mm Hg on day 38 after aortic banding and thereafter gradually decreased to 124±7 mm Hg on day 56 after aortic banding (n=3 for each; see the online data supplement for details).

Salt Sensitivity in Sham Mice and AB Mice

High salt intake did not increase U-NE or U-E excretion in Sham mice (Figure 3A). In AB mice, however, high salt intake significantly increased U-NE and U-E excretion. Furthermore, U-NE excretion in AB mice began to increase within 5 days (AB-Hd5 mice) of beginning the high-salt diet (Figure 3A), although cardiac function was preserved (%FS 43±1%; n=5). ICV infusion of regular-Na aCSF did not significantly increase U-NE or U-E excretion in Sham mice or AB mice (Figure 3B). ICV infusion of high-Na aCSF significantly increased U-NE and U-E excretion in both Sham mice and AB mice. The increase in U-NE excretion in AB mice, however, tended to be greater than that in Sham mice ($P=0.1$), and the increase in U-E excretion was significantly greater in AB mice than in Sham mice (Figure 3B).

In the acute experiments, high-Na aCSF ICV infusion increased arterial pressure and heart rate in both Sham-4 mice and AB-4 mice, but the degree of these changes was significantly greater in AB-4 mice (Figure 3C). The pressor response to angiotensin II ICV infusion was greater in AB-4 mice than Sham-4 mice (ΔMAP 8.6±1.2 mm Hg in Sham-4, 22.3±3.4 mm Hg in AB-4 mice, n=4 for each), however, the pressor response to carbachol ICV infusion did not differ between groups (ΔMAP: 9.5±1.8 mm Hg in Sham-4, 13.7±1.5 mm Hg in AB-4 mice; n=4 for each).

Na concentration in the brain tissues (circumventricular tissues including hypothalamus) was higher in AB-H mice than in the other groups (AB-H, 116±2 ppm; AB-R, 102±4 ppm; Sham-R, 104±2 ppm; Sham-H, 104±2 ppm; n=5 for each; $P<0.05$).

Effects of High-Na aCSF ICV Infusion on Cardiac Function

In AB mice, high-Na aCSF ICV infusion significantly increased LVDD (3.4±0.4 mm) and decreased %FS (32±1%) compared with regular-Na aCSF ICV infusion (LVDD, 3.2±0.5 mm; %FS, 41±1%; n=5 for each; $P<0.05$). Arterial pressure did not differ between AB mice with high-Na aCSF and regular-Na aCSF (94±3 mm Hg in high-Na aCSF,

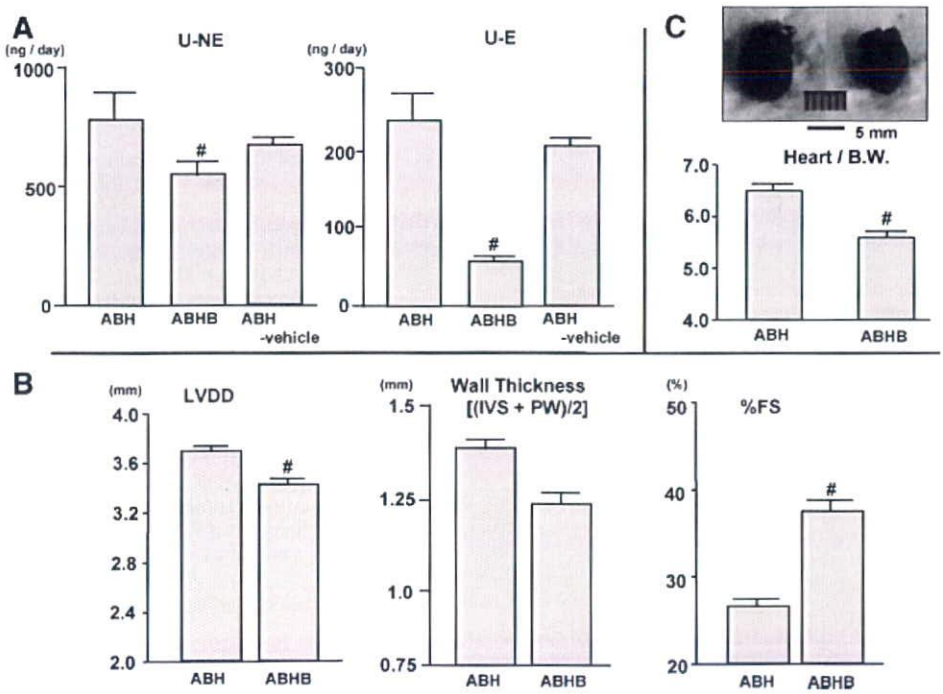

Figure 4. A, The 24-hour U-NE and U-E excretion in each group after ICV benzamil (AB-HB) infusion. #$P<0.05$ vs AB-H (n=5 to 10). B, Cardiac function evaluation by echocardiography in each group. IVS indicates interventricular septum; PW, posterior wall. #$P<0.05$ vs AB-H (n=8 in each group). C, Relative heart weight in each group. #$P<0.05$ vs AB-H (n=6 in each group).

101±5 mm Hg in regular-Na aCSF; n=4 for each). In Sham mice, high-Na aCSF ICV infusion had no significant effects on cardiac function compared with regular-Na aCSF ICV infusion (LVDD, 3.1±0.2 mm in high-Na aCSF versus 3.1±0.3 mm in regular-Na aCSF; %FS, 46±2% in high-Na aCSF versus 48±3% in regular-Na aCSF; n=5 for each).

Effects of ENaC Blocker ICV Infusion on Cardiac Function

In comparison with AB-H mice, ICV infusion of the ENaC blocker benzamil (AB-HB mice) significantly decreased U-NE and U-E excretion (Figure 4A). Cardiac function (LVDD and %FS) significantly improved in AB-HB mice compared with AB-H mice (Figure 4B). Relative heart weight decreased in AB-HB mice compared with AB-H mice (Figure 4C). Arterial pressure was significantly higher and heart rate was lower in AB-HB mice than in AB-H mice (Online Table II). ICV infusion of benzamil did not affect these measures in AB-R mice, and ICV infusion of vehicle in AB-H mice also did not significantly decrease U-NE and U-E excretion (data not shown).

Rho-Kinase Activity and AT_1R Expression in the Brain

The amount of AT_1R and the expression of p-moesin, a substrate of Rho-kinase, in the brain stem and circumventricular tissue were significantly higher in AB-4 mice than in Sham-4 mice (Figure 5).

Effects of ICV Infusion of Rho-Kinase Inhibitor and AT_1R Blocker on Cardiac Function

In comparison with AB-H mice, ICV infusion of the Rho-kinase inhibitor Y-27632 (AB-HY mice) or AT_1R blocker telmisartan (AB-HT mice) induced a significant decrease in U-NE and U-E excretion (Figure 6A). In AB-HT mice, U-NE and U-E decreased in a dose-related manner. Cardiac function was also significantly improved in AB-HY mice or AB-HT mice compared with AB-H mice (Figure 6B). Relative heart weight was decreased in AB-HY mice or AB-HT mice compared with AB-H mice (Figure 6C). Heart rate was significantly decreased in AB-HY mice or AB-HT mice compared with AB-H mice (Online Table II). Infusion of vehicle (aCSF or DMSO) did not have these effects.

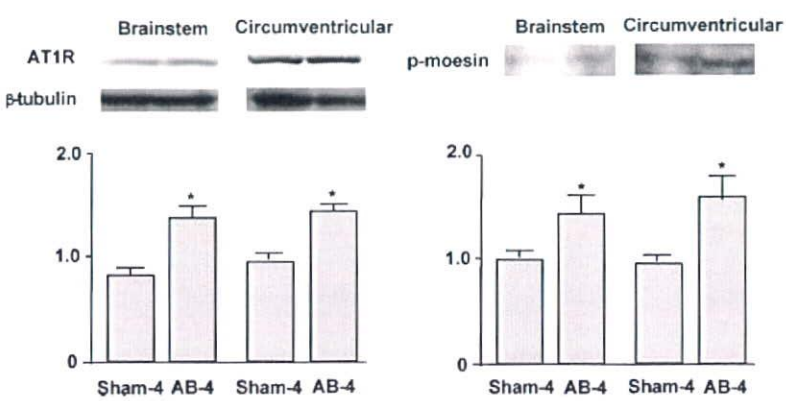

Figure 5. Left, Representative Western blots demonstrating the expression of AT_1R in the brain (circumventricular tissues including hypothalamus and brain stem tissues) of Sham-4 or AB-4. The graph shows the means for the quantification of 4 separate experiments. Data are expressed as the relative ratio to β-tubulin expression (n=4 in each group). *$P<0.05$ vs Sham-4. Right, Representative Western blot demonstrating the expression of p-moesin, a substrate of Rho-kinase in the brain (circumventricular tissues including hypothalamus and brain stem tissues) of Sham-4 or AB-4. The graph shows the means for the quantification of 3 separate experiments. Data are expressed as the relative ratio to Sham-4, which was assigned a value of 1 (n=3 in each group). *$P<0.05$ vs Sham.

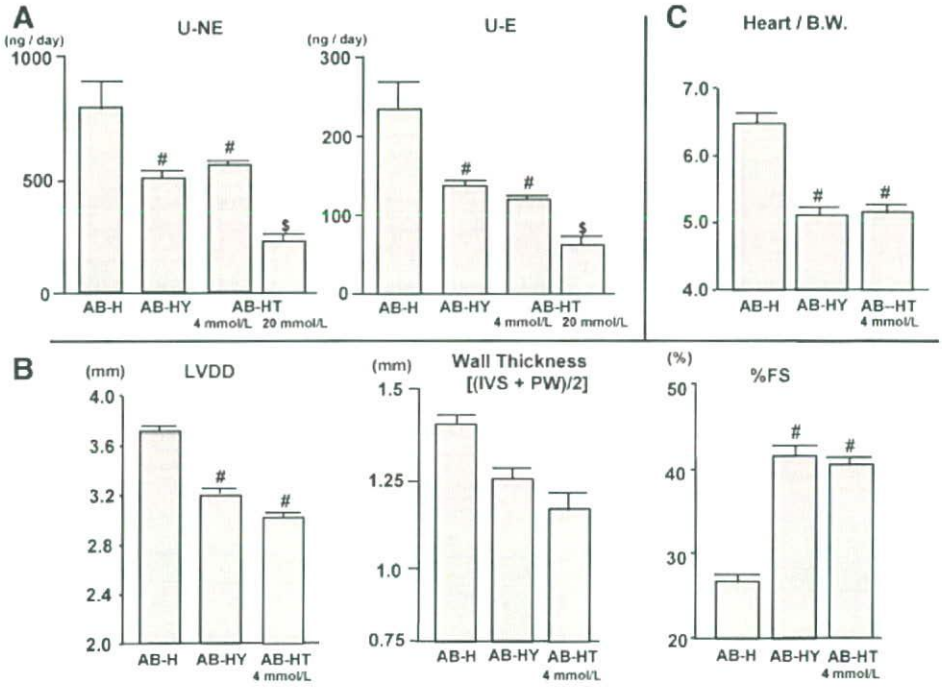

Figure 6. A, The 24-hour U-NE and U-E excretion in each group after Y-27632 (AB-HY) or telmisartan (AB-HT) ICV infusion. #$P<0.05$ vs AB-H (n=5 to 10), \$$P<0.05$ vs AB-HT 4 mmol/L. B, Cardiac function evaluation by echocardiography in each group after Y-27632 (AB-HY) or telmisartan (AB-HT) ICV infusion. IVS indicates interventricular septum; PW, posterior wall. #$P<0.05$ vs AB-H (n=5 to 8). C, Relative heart weight in each group after Y-27632 (AB-HY) or telmisartan (AB-HT) ICV infusion. #$P<0.05$ vs AB-H (n=5 to 6).

Serum Parameters

Serum Na concentration did not differ between groups (Sham-4, 151±2 mEq/L; AB-4, 151±1 mEq/L; AB-R, 150±1 mEq/L; AB-H, 152±1 mEq/L). Serum creatinine concentration, as a marker of renal function, also did not differ between groups (Sham-4, 0.11±0.01 mg/dL; AB-4, 0.09±0.01 mg/dL; AB-R, 0.12±0.01 mg/dL; AB-H, 0.11±0.01 mg/dL). Serum aldosterone levels were not different between Sham-4 and AB-4 mice and were significantly lower in AB-H mice than in AB-4 mice, AB-R mice, and Sham-4 mice (Sham-4, 120±11 pg/dL; AB-4, 145±28 pg/dL; AB-R, 163±17 pg/dL; AB-H, 54±6 pg/dL; n=6 to 7; $P<0.05$).

Discussion

The major findings of the present study were that mice with pressure overload produced by aortic banding acquired brain Na sensitivity via the activation of brain ENaCs through stimulation of the Rho/Rho-kinase pathway and RAS. Because of the acquired brain Na sensitivity, high salt intake led to sympathetic activation, which led to the deterioration of cardiac function. These findings are novel and suggest new targets for studies of the prevention and treatment of cardiac deterioration in patients with pressure overload, such as hypertensive heart disease.

The most important finding of the present study was that the mice with pressure overload acquired brain Na sensitivity and a high-salt diet increased the sympathetic outflow before cardiac dysfunction was detected. In AB-4 mice, only LVWT tended to increase compared to the Sham-4 mice, but there was no effect on cardiac function. Both a high-salt and regular-salt diet for an additional 4 weeks, however, induced cardiac dysfunction in AB mice compared with Sham mice. Furthermore, AB mice on the high-salt diet exhibited significantly more severe cardiac dysfunction and greater activation of the sympathetic system than AB mice on the regular-salt diet. This high-salt induced enhanced sympathetic drive was obvious before cardiac function was impaired. In Sham mice, a high salt intake did not increase U-NE and U-E excretion and had no effect on cardiac function. These results strongly suggest that the mice with pressure overload acquired the salt sensitivity before cardiac function began to deteriorate and that a high salt intake augmented cardiac dysfunction by inducing sympathetic activation.

To clarify the contribution of central mechanisms to the acquisition of salt sensitivity in mice with pressure overload, we examined the effects of high-Na in the CSF on sympathetic activity and arterial pressure after ICV infusion of high-Na or regular-Na aCSF. Compared with ICV infusion of regular-Na aCSF, high-Na aCSF induced significant increases in U-NE and U-E excretion in both groups of mice. The increased U-NE excretion in AB mice, however, tended to be greater than that in Sham mice ($P=0.1$), and the increase in U-E excretion was significantly greater in AB mice than in Sham mice. Furthermore, ICV infusion of high-Na aCSF induced significantly greater increases in arterial pressure and heart rate in AB-4 mice than in Sham-4 mice. To assess the specificity of the pressure response to a high-Na ICV infusion, we examined the response to other central stimuli, such as angiotensin II and carbachol. The response to angiotensin II was greater in AB-4 mice than Sham-4 mice. In contrast, the response to carbachol was not different between groups. The effect of the angiotensin II ICV infusion was supported by the findings that the extent of brain AT_1R was greater in AB-4 mice than Sham-4 mice, and the effect of carbachol ICV infusion indicated the specific activation of the brain RAS and Na sensing system. Together with the findings from the systemic salt loading, our findings suggest that the acquisition of Na sensitivity in the brain of

mice with pressure overload results from two different mechanisms: (1) the enhancement of Na uptake into the brain and (2) the increase in responsiveness to Na within the brain.

Another important finding of the present study was the high-Na aCSF-induced activation of the sympathetic system, which further deteriorates cardiac function in mice with pressure overload. There are some reports that enhanced sympathetic drive plays an important role in the progression of heart failure.[20,21] In the present study, in comparison with ICV infusion of regular-Na aCSF, high-Na aCSF induced a significant decline in cardiac function. To evaluate the possibility that the increase in the afterload induced by increased arterial pressure affected cardiac function, we measured arterial pressure 2 weeks after ICV infusion of high-Na aCSF and confirmed that arterial pressure did not significantly increase compared with regular-Na ICV infusion. These results suggest that high-Na aCSF-induced sympathetic hyperactivation may lead to cardiac dysfunction in mice with pressure overload and the deterioration of cardiac function may not be attributable to the increase in the afterload induced by the arterial pressure elevation. However, high-salt loading caused further decreases in cardiac function in AB mice, indicating that high-salt loading may induce further decrease in cardiac function both by sympathetic activation and an increase in arterial pressure in AB mice.

Arterial pressure in AB-4 mice was significantly higher than that in Sham-4 mice; and arterial pressure in AB-H 1-week mice, which were loaded with a high-salt diet for 1 week, was further increased compared with that in AB-4 mice. Arterial pressure in AB-R mice and AB-H mice decreased to levels similar or lower than that in Sham mice within 8 weeks. This may relate to cardiac dysfunction. In fact, the LVEDP in AB-H mice was significantly greater than that in AB-R or Sham-R mice and the LV %FS in AB-H mice was significantly smaller than that in AB-R or Sham-R mice. To validate the arterial pressure measurements, we measured arterial pressure and heart rate using a radio-telemetry system with mice in the awake state. At day 28 after aortic banding (AB-4 mice), arterial pressure was significantly higher than that before aortic banding. Thereafter, in AB-H mice, arterial pressure was significantly further increased at day 35 (1 week after the starting high-salt diet), but the general health of the mice deteriorated, likely because of severe lung congestion, which was supported by the high lung/body weight ratio. In AB-R mice, arterial pressure peaked at around day 40 and then gradually decreased. Implantation of the telemetry catheter in the carotid artery might further augment the pressure overload and induce severe lung congestion in AB-H mice. Therefore, we examined the arterial pressure under anesthesia in acute experiments. The findings indicate that aortic banding causes a pressure overload for LV and high-salt loading superimposed on aortic banding further augments the pressure overload.

To explore the mechanisms of the acquisition of brain Na sensitivity, we examined the effects of an ENaC blocker, benzamil. Brain ENaCs are involved in the high salt–induced increase in central sympathetic outflow in salt-sensitive hypertensive rats.[1,3] In the present study, brain ENaC blockade by benzamil attenuated the high salt–induced activation of the sympathetic nervous system and the deterioration of cardiac function. Furthermore, we examined the brain Na concentrations in each group. We were unable to measure Na concentrations in the CSF in the present study, because in mice it is difficult to obtain the volume of CSF required to measure Na concentration. Therefore, we measured the Na concentrations in the brain tissues and confirmed that AB-H mice had higher Na concentrations than the other groups. These findings support our hypothesis that the pressure overload activates brain ENaCs and augments Na transport from plasma to the CSF, resulting in sympathoexcitation. However, we did not examine the effects of brain ENaCs on Na transport directly and ENaCs have both epithelial and neural components.[11] Therefore, it is possible that the benzamil may affect ENaCs on neural components and cause sympathoinhibitory effects. The role of ENaCs on neural components in sympathetic modulation remains unclear. A similar dose of benzamil was used as specific ENaC blocker in previous studies,[4] and the estimated benzamil concentration in the CSF in the present study was considered to be specific for ENaCs (<100 nmol/L).[22–24] Therefore, the dose of benzamil used in the present study was adequate for use as a specific ENaC blocker. Further studies are required to measure ENaC activity directly. Although some studies have demonstrated that salt intake induces sympathoexcitation via central mechanisms[1–3] and the effects of brain ENaCs on cardiac function,[4] these previous studies used genetic models of salt-sensitive hypertension or heart failure induced by myocardial infarction, whereas we used the pressure overload produced by aortic banding model in mice without a genetic background of salt sensitivity.

Finally, we focused on Rho-kinase and angiotensin II as the mechanisms involved in brain ENaC activation in the mice with pressure overload, because ENaCs in kidney are reported to be activated by Rho-kinase[12] and angiotensin II.[13] In addition, we recently reported that Rho-kinase[16,25–27] and angiotensin II[28] in the brain contribute to cardiovascular regulation via the sympathetic nervous system. In the present study, we confirmed that compared to Sham-4 mice, the brains of AB-4 mice had higher levels of AT_1R and higher Rho-kinase activity, and blockade of either AT_1R or Rho-kinase attenuates high salt–induced sympathetic activation and cardiac dysfunction. These findings suggest that enhanced brain Na sensitivity results from the activation of brain ENaCs via the Rho/Rho-kinase pathway and RAS in mice with pressure overload. However, ENaCs may be upstream of RAS in brain.[29] In the present study, we did not address this issue. Further studies are needed to clarify the relationship between RAS and ENaCs in brain. It is possible that renal blood flow is reduced in mice with suprarenal abdominal aortic banding, resulting in renal dysfunction[30] concomitant with activation of the systemic RAS.[31] It is unlikely that this occurred in the present study because we confirmed that serum creatinine and aldosterone levels were not significantly different between groups and the mean arterial pressure in the AB-4 mice measured from the right femoral artery was above 90 mm Hg, suggesting that the aortic banding procedure did not significantly reduce renal blood flow and impair renal function. Previous studies

demonstrated that excess stimulation of cardiopulmonary and arterial baroreceptors impair baroreflex function[32,33] and RAS[32] or Rho-kinase[33] in the brain might contribute to the impaired baroreflex function. In the present study, we demonstrated that arterial pressure measured from the carotid artery and LVEDP were significantly greater in AB-4 mice than in Sham-4 mice. The excess stimulation of cardiopulmonary and arterial baroreceptor may contribute to the activation of the Rho/Rho-kinase pathway and RAS in the brains of the mice with pressure overload, even before high-salt loading.

In conclusion, the present findings strongly suggest that mice with pressure overload acquire brain Na sensitivity because of the activation of brain ENaCs via the Rho/Rho-kinase pathway and RAS. The acquired brain Na sensitivity contributes to high salt–induced sympathetic activation, leading to deteriorating cardiac function in mice with pressure overload.

Sources of Funding

This work was supported by Grants-in-Aid for Scientific Research from the Japan Society for the Promotion of Science (B19390231 and 19890148) and the Mitsubishi Pharma Research Foundation.

Disclosures

None.

References

1. Nishimura M, Ohtsuka K, Nanbu A, Takahashi H, Yoshimura M. Benzamil blockade of brain Na^+ channels averts Na^+-induced hypertension in rats. *Am J Physiol*. 1998;274:R635–R644.
2. Fujita M, Ando K, Nagae A, Fujita T. Sympathoexcitation by oxidative stress in the brain mediates arterial pressure elevation in salt-sensitive hypertension. *Hypertension*. 2007;50:360–367.
3. Huang BS, Amin MS, Leenen FHH. The central role of the brain in salt-sensitive hypertension. *Curr Opin Cardiol*. 2006;21:295–304.
4. Huang BS, Leenen FHH. Blockade of brain mineralcorticoid receptors or Na^+ channels prevents sympathetic hyperactivity and improve cardiac function in rats post-MI. *Am J Physiol*. 2005;288:H2491–H2497.
5. Leenen FHH. Brain mechanisms contributing to sympathetic hyperactivity and heart failure. *Circ Res*. 2007;101:221–223.
6. Mark AL. Sympathetic dysregulation in heart failure: mechanisms and therapy. *Clin Cardiol*. 1995;18:I3–I8.
7. Zucker IH. Novel mechanisms of sympathetic regulation in chronic heart failure. *Hypertension*. 2006;48:1005–1011.
8. Takimoto E, Champion HC, Li M, Belardi D, Ren S, Rodriguez ER, Bedja D, Gabrielson KL, Wang Y, Kass DA. Chronic inhibition of cyclic phosphodiesterase 5A prevents and reverse cardiac hypertrophy. *Nat Med*. 2005;11:214–222.
9. Klotz S, Hay I, Zhang G, Maurer M, Wang J, Burkhoff D. Development of heart failure in chronic hypertensive Dahl rats focus on heart failure with preserved ejection fraction. *Hypertension*. 2006;47:901–911.
10. Vigne P, Champigny G, Marsaut R, Barbry P, Frelin C, Lazdunski M. A new type of amiloride-sensitive cation channel in endothelial cells of brain microvessels. *J Biol Chem*. 1989;264:7663–7668.
11. Amin MS, Wang HW, Reza E, Whitman SC, Tuana BS, Leenen FHH. Distribution of epithelial sodium channels and mineralocorticoid receptors in cardiovascular regulatory centers in rat brain. *Am J Physiol*. 2005;289:R1787–R1797.
12. Pochynyuk O, Medina J, Gamper N, Genth H, Stockand JD, Staruschenko A. Rapid translocation and insertion of the epithelial Na^+ channel in response to RhoA signaling. *J Biol Chem*. 2006;281:26520–26527.
13. Peti-Peterdi J, Warnock DG, Bell PD. Angiotensin II directly stimulates ENaC activity in the cortical collecting duct via AT1 receptors. *J Am Soc Nephrol*. 2002;13:1131–1135.
14. Harada K, Komuro I, Shiojima I, Hayashi D, Kudoh S, Mizuno T, Kijima K, Matsubara H, Sugaya T, Murakami K, Yazaki Y. Pressure overload induces cardiac hypertrophy in angiotensin II type II 1A receptor knockout mice. *Circulation*. 1998;97:1952–1959.
15. Sakai K, Hirooka Y, Shigematsu H, Kishi T, Ito K, Shimokawa H, Takeshita A, Sunagawa K. Overexpression of eNOS in brain stem reduces enhanced sympathetic drive in mice with myocardial infarction. *Am J Physiol Heart Circ Physiol*. 2005;289:H2159–H2166.
16. Ito K, Kimura Y, Hirooka Y, Sagara Y, Sunagawa K. Activation of Rho-kinase in the brainstem enhances sympathetic drive in mice with heart failure. *Auton Neurosci*. 2008;142:77–81.
17. Wirth A, Benyó Z, Lukasova M, Leutgeb B, Wettschureck N, Gorbey S, Örsy P, Horváth B, Maser-Gluth C, Greiner E, Lemmer B, Schütz G, Gutkind S, Offermanns S. G_{12}-G_{13}-LARG-mediated signaling in vascular smooth muscle is required for salt-induced hypertension. *Nat Med*. 2008;14:64–68.
18. Uehata M, Ishizaki T, Satoh H, Ono T, Kawahara T, Morishita T, Tamakawa H, Yamagami K, Inui J, Maekawa M, Narumiya S. Calcium sensitization of smooth muscle mediated by a Rho-associated protein kinase in hypertension. *Nature*. 1997;389:990–994.
19. Matsui T, Maeda M, Doi Y, Yonemura S, Amano M, Kaibuchi K, Tsukita S. Rho-kinase phosphorylate COOH-terminal threonines of ezrin/radixin/moesin (ERM) proteins and regulates their head-to-tail association. *J Cell Biol*. 1998;140:647–657.
20. Cohn JN, Levine TB, Olivari MT, Garberg V, Lura D, Francis GS, Simon AB, Rector T. Plasma norepinephrine as a guide to prognosis in patients with chronic congestive heart failure. *N Engl J Med*. 1984;311:819–823.
21. Rector TS, Olivari MT, Levine TB, Francis GS, Cohn JN. Predicting survival for an individual with congestive heart failure using the plasma norepinephrine concentration. *Am Heart J*. 1987;114:148–152.
22. Teiwes J, Toto RD. Epithelial sodium channel inhibition in cardiovascular disease. *Am J Hypertens*. 2007;20:109–117.
23. Hirsh AJ, Sabater JR, Zamurs A, Smith RT, Paradiso AM, Hopkins S, Abraham WM, Boucher RC. Evaluation of second generation amiloride analogs as therapy for cystic fibrosis lung disease. *J Pharmacol Exp Ther*. 2004;311:929–938.
24. Rudick RA, Zirretta DK, Herndon RM. Clearance of albumin from mouse subarachnoid space: a measure of CSF bulk flow. *J Neurosci Methods*. 1982;6:253–259.
25. Ito K, Hirooka Y, Sakai K, Kishi T, Kaibuchi K, Shimokawa H, Takeshita A. Rho/Rho-kinase pathway in brain stem contributes to blood pressure regulation via sympathetic nervous system: possible involvement in neural mechanisms of hypertension. *Circ Res*. 2003;92:1337–1343.
26. Ito K, Hirooka Y, Kishi T, Kimura Y, Kaibuchi K, Shimokawa H, Takeshita A. Rho/Rho-kinase pathway in the brainstem contributes to hypertension caused by chronic nitric oxide synthase inhibition. *Hypertension*. 2004;43:156–162.
27. Ito K, Hirooka Y, Kimura Y, Sagara Y, Sunagawa K. Ovariectomy augments hypertension through Rho-kinase activation in the brain stem in female spontaneously hypertensive rats. *Hypertension*. 2006;48:651–657.
28. Sagara Y, Hirooka Y, Nozoe M, Ito K, Kimura Y, Sunagawa K. Pressor response induced by central angiotensin II is mediated by activation of Rho/Rho-kinase pathway via AT_1 receptors. *J Hypertens*. 2007;25:399–406.
29. Huang BS, Cheung WJ, Wang Hao, Tan J, White RA, Leenen FHH. Activation of brain renin-angiotensin-aldosterone system by central sodium in Wister rats. *Am J Physiol*. 2006;291:H1109–H1117.
30. Akers WS, Cross A, Speth R, Dwoskin LP, Cassis LA. Renin-angiotensin system andsympathetic nervous system in cardiac pressure-overload hypertrophy. *Am J Physiol*. 2000;279:H2797–H2806.
31. Héliés-Toussaint C, Moinard C, Rasmusen C, Tabbi-Anneni I, Cynober L, Gryngerg A. Aortic banding in rats as a model to investigate malnutrition associated with heart failure. *Am J Physiol*. 2005;288:R1325–R1331.
32. Wang WZ, Gao L, Pan YX, Zucker IH, Wang W. AT1 receptor in the nucleus tractus solitarii mediate the interaction between the baroreflex and the cardiac sympathetic afferent reflex in anesthetized rats. *Am J Physiol*. 2007;292:R1137–R1145.
33. Ito K, Hirooka Y, Sagara Y, Kimura Y, Kaibuchi K, Shimokawa H, Takeshita A, Sunagawa K. Inhibition of Rho-kinase in the brainstem augments baroreflex control of heart rate in rats. *Hypertension*. 2004;44:478–483.

Circ J 2009; **73:** 851–859

Servo-Controlled Hind-Limb Electrical Stimulation for Short-Term Arterial Pressure Control

Toru Kawada, MD; Shuji Shimizu, MD; Hiromi Yamamoto, MD*;
Toshiaki Shishido, MD; Atsunori Kamiya, MD; Tadayoshi Miyamoto, PhD**;
Kenji Sunagawa, MD†; Masaru Sugimachi, MD

Background: Autonomic neural intervention is a promising tool for modulating the circulatory system thereby treating some cardiovascular diseases.

Methods and Results: In 8 pentobarbital-anesthetized cats, it was examined whether the arterial pressure (AP) could be controlled by acupuncture-like hind-limb electrical stimulation (HES). With a 0.5-ms pulse width, HES monotonically reduced AP as the stimulus current increased from 1 to 5 mA, suggesting that the stimulus current could be a primary control variable. In contrast, the depressor effect of HES showed a nadir approximately 10 Hz in the frequency range between 1 and 100 Hz. Dynamic characteristics of the AP response to HES approximated a second-order low-pass filter with dead time (gain: −10.2±1.6 mmHg/mA, natural frequency: 0.040±0.004 Hz, damping ratio 1.80±0.24, dead time: 1.38±0.13 s, mean±SE). Based on these dynamic characteristics, a servo-controlled HES system was developed. When a target AP value was set at 20 mmHg below the baseline AP, the time required for the AP response to reach 90% of the target level was 38±10 s. The steady-state error between the measured and target AP values was 1.3±0.1 mmHg.

Conclusions: Autonomic neural intervention by acupuncture-like HES might provide an additional modality to quantitatively control the circulatory system. (*Circ J* 2009; **73:** 851–859)

Key Words: Proportional-integral controller; Transfer function

Because abnormality in the autonomic nervous system is often associated with cardiovascular diseases, treating cardiovascular diseases by autonomic neural interventions have attracted many researchers![1–6] Recently, autonomic neural interventions using electronic devices have again gained the focus of attention as a potential modality for treating cardiovascular diseases resistant to conventional therapeutics. To name a few, chronic vagal nerve stimulation dramatically improves the survival of chronic heart failure after myocardial infarction in rats![7] Chronic baroreceptor activation enhances the survival of pacing-induced heart failure in dogs![8] A recent version of a device-based treatment of hypertension in human is reported![9] A framework of electrical neural intervention is also effective to elevate arterial pressure (AP) against hypotensive events![10–13]

Aside from direct neural stimulation, electroacupuncture can modify autonomic balance, thereby treating cardiovascular diseases![14–16] Although one feature of the electroacupuncture might be its long-lasting effects, immediate cardiovascular responses to acupuncture-like stimulation are also observed in several experimental settings. For example, a 60-s manual acupuncture-like stimulation of a hind limb reduces renal or cardiac sympathetic nerve activity, causing hypotension and bradycardia in anesthetized rats![17,18] We have shown that electrical stimulation of a hind limb using acupuncture needles immediately resets the arterial baroreflex and reduces sympathetic nerve activity in anesthetized rabbits![19] Acupuncture-like hind-limb electrical stimulation (HES) induces immediate hypotension with changes in the relationship between cardiac and renal sympathetic nerve activities in anesthetized cats![20]

In the present study, we hypothesized that AP could be controlled by HES. Quantification of the dynamic input–output relationship between a given stimulus and the AP response is essential for artificially controlling AP![10–12] Accordingly, the first aim was to identify the dynamic input–output relationship between HES and the AP response. The second aim was to develop a feedback controller system that could reduce AP at a prescribed target level using HES.

Methods

Surgical Preparation

Animal care was provided in strict accordance with the *Guiding Principles for the Care and Use of Animals in the Field of Physiological Sciences,* approved by the Physiological Society of Japan. All protocols were approved by the Animal Subject Committee of the National Cardiovascular Center. Eight adult cats weighing from 2.3 to 4.3 kg were

(Received November 17, 2008; revised manuscript received December 10, 2008; accepted December 21, 2008; released online March 18, 2009)

*Department of Cardiovascular Dynamics, Advanced Medical Engineering Center, National Cardiovascular Center Research Institute, Suita, *Division of Cardiology, Department of Internal Medicine, Kinki University School of Medicine, Osakasayama, **Department of Physical Therapy, Faculty of Health Sciences, Morinomiya University of Medical Sciences, Osaka and †Department of Cardiovascular Medicine, Graduate School of Medical Sciences, Kyushu University, Fukuoka, Japan*

Mailing address: Toru Kawada, MD, Department of Cardiovascular Dynamics, Advanced Medical Engineering Center, National Cardiovascular Center Research Institute, 5-7-1 Fujishirodai, Suita 565-8565, Japan. E-mail torukawa@res.ncvc.go.jp

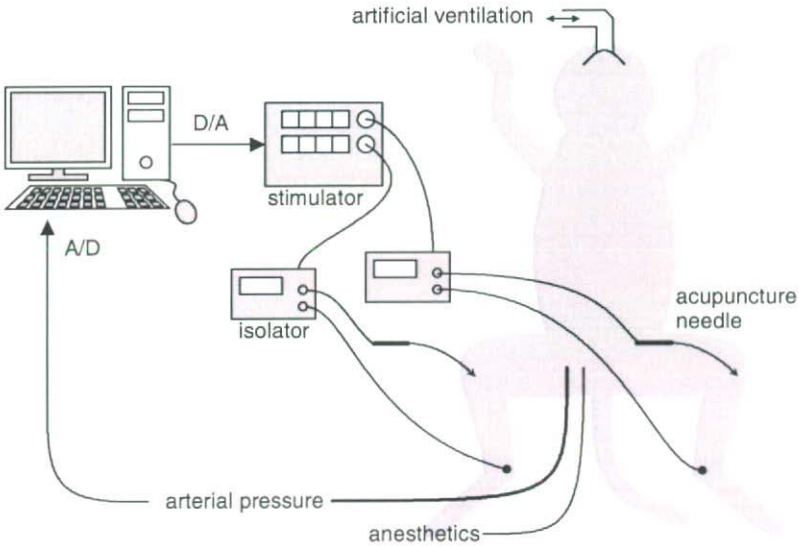

Figure 1. Experimental setup.

anesthetized by an intraperitoneal injection of pentobarbital sodium (30–35 mg/kg) and ventilated mechanically via a tracheal tube with oxygen-supplied room air. The depth of anesthesia was maintained with a continuous intravenous infusion of pentobarbital sodium (1–2 $mg \cdot kg^{-1} \cdot h^{-1}$) through a catheter inserted into the right femoral vein. Vecuronium bromide (0.5–1.0 $mg \cdot kg^{-1} \cdot h^{-1}$, iv) was given continuously to suppress muscular activity. AP was measured using a catheter-tip manometer inserted from the right femoral artery and advanced into the thoracic aorta.

HES

In the supine position, both hind limbs were lifted to obtain a better view of the lateral sides of the lower legs. An acupuncture needle with a diameter of 0.2 mm (CE0123, Seirin-Kasei, Shimizu, Japan) was inserted into a point below the knee joint just lateral to the tibia[20] A 23-gauge needle was inserted into the skin behind the ankle as the ground. HES was applied bilaterally via 2 independent isolators connected to an electrical stimulator (SEN 7203, Nihon Kohden, Tokyo, Japan) as shown in **Figure 1**. The pulse width was changed manually whereas the stimulus frequency and the stimulus current were controlled by a dedicated laboratory computer system. The electrical stimulation was started after the hemodynamic effects of needle insertion had disappeared, and the acupuncture needle remained inserted during each protocol.

Protocols

Protocol 1 (n=8) To quantify the AP response to HES as a function of stimulus current and pulse width, we fixed the stimulus frequency at 10 Hz and changed the stimulus current stepwise from 0 to 5 mA in 1-mA increments every minute. The 6-min current test was repeated with an intervening interval of 3–5 min using different pulse widths (0.1, 0.2, 0.5 and 1 ms). The order of the pulse-width settings was randomized across the animals.

Protocol 2 (n=8) To quantify the AP response to HES as a function of stimulus frequency and pulse width, we fixed the stimulus current at 3 mA and changed the stimulus frequency sequentially from 0 to 100 Hz (0, 1, 2, 5, 10, 15, 20, 50 and 100 Hz). Each stimulus frequency was maintained for 1 min. The 9-min frequency test was repeated with an intervening interval of 3–5 min using different pulse widths (0.1, 0.2, 0.5 and 1 ms). The order of the pulse-width settings was randomized across the animals.

Protocol 3 (n=8) To identify the dynamic input–output relationship between HES and the AP response, we randomly turned HES on and off every 2 s according to a binary white noise sequence for 30 min. The HES setting (0.5-ms pulse width, 10 Hz, 3 mA) was chosen to induce effective hypotension based on the preliminary results obtained from Protocols 1 and 2.

Protocol 4 (n=8) Based on the result of Protocol 3, we designed a feedback controller that could automatically adjust the stimulus frequency and the stimulus current for HES. The pulse width was fixed at 0.5 ms. To examine the performance of the feedback controller, we set a target AP value at 20 mmHg below the baseline AP and activated the feedback controller for 10 min.

The following 2 supplemental protocols were performed in 3 of the 8 cats: (1) we inserted 2 acupuncture needles into the triceps surae muscle with a distance of approximately 2.5 cm, and examined if changes in AP was associated with direct muscle stimulation (0.5-ms pulse width, 10 Hz, 3 mA). Both hind limbs were stimulated simultaneously using 2 independent isolators; and (2) we exposed the sciatic nerve after finishing Protocols 1 through 4, and examined if sectioning the sciatic nerve abolished the hemodynamic effects of HES. Unilateral HES was performed (0.5-ms pulse width, 10 Hz, 3 mA) before and after sectioning the ipsilateral sciatic nerve.

Data Analysis

In Protocols 1 and 2, the AP value was obtained by averaging the last 10-s data at each stimulus condition. In Protocol 1, the effect of stimulus current was assessed by changes in AP from the 0-mA stimulus condition for each pulse width. In Protocol 2, the effect of stimulus frequency was assessed by changes in AP from the 0-Hz stimulus condition for each pulse width.

In Protocol 3, the transfer function from HES to AP was estimated by means of an analysis for one-input, one-output systems. Data were first resampled at 10 Hz and segmented into 8 sets of 50%-overlapping bins of 4,096 points each. For each segment, a linear trend was subtracted and a

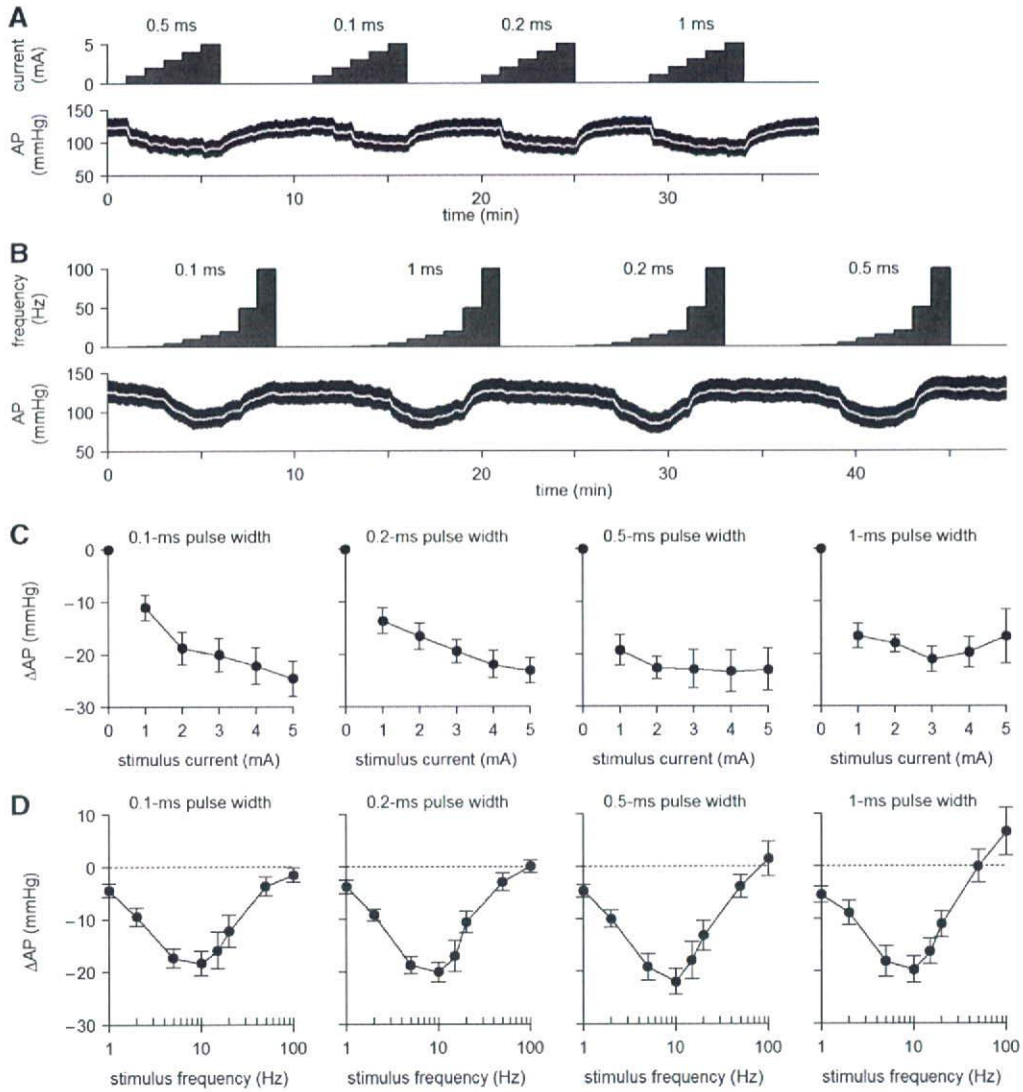

Figure 2. (**A**) Typical recordings of Protocol 1 showing the effects of stimulus current and pulse width on arterial pressure (AP). (**B**) Typical recordings of Protocol 2 showing the effects of stimulus frequency and pulse width on AP. The white lines in the AP traces indicate 2-s moving averaged data. (**C**) Changes in AP as a function of the stimulus current. AP decreased monotonously as the stimulus current increased ($P<0.05$). (**D**) Changes in AP as a function of the stimulus frequency. AP decreased more as the stimulus frequency increased from 1 to 10 Hz but the depressor effect became smaller when the stimulus frequency exceeded 10 Hz ($P<0.05$).

Hanning window was applied. Frequency spectra of the input and output were obtained via fast Fourier transformation. Next, the ensemble averages of input power spectral density [$Sxx(f)$], output power spectral density [$Syy(f)$], and cross spectral density between the input and output [$Syx(f)$] were calculated over the 8 segments. Finally, the transfer function from input to output [$H(f)$] was calculated as:[21]

$$H(f)=\frac{Syx(f)}{Sxx(f)} \quad (1)$$

To quantify the linear dependence between the input and output signals in the frequency domain, a magnitude-squared coherence function [$Coh(f)$] was also calculated as:[21]

$$Coh(f)=\frac{|Syx(f)|^2}{Sxx(f)Syy(f)} \quad (2)$$

In Protocol 4, the performance of the feedback controller was evaluated by the time required for the AP response to reach 90% of the target AP decrease and by the standard deviation of the steady-state error between the target and measured AP values during the last 5 min of the 10-min feedback control. These 2 values were calculated based on the 2-s moving averaged data of AP.

Statistical Analysis

All data are presented as mean and SE values. In Protocol 1, changes in AP were examined by 2-way repeated-measures analysis of variance (ANOVA) using the stimulus current as one factor and the pulse width as the other factor.[22] In Protocol 2, changes in AP were examined by 2-way repeated-measures ANOVA using the stimulus frequency as one factor and the pulse width as the other factor. Differences were considered significant when $P<0.05$.

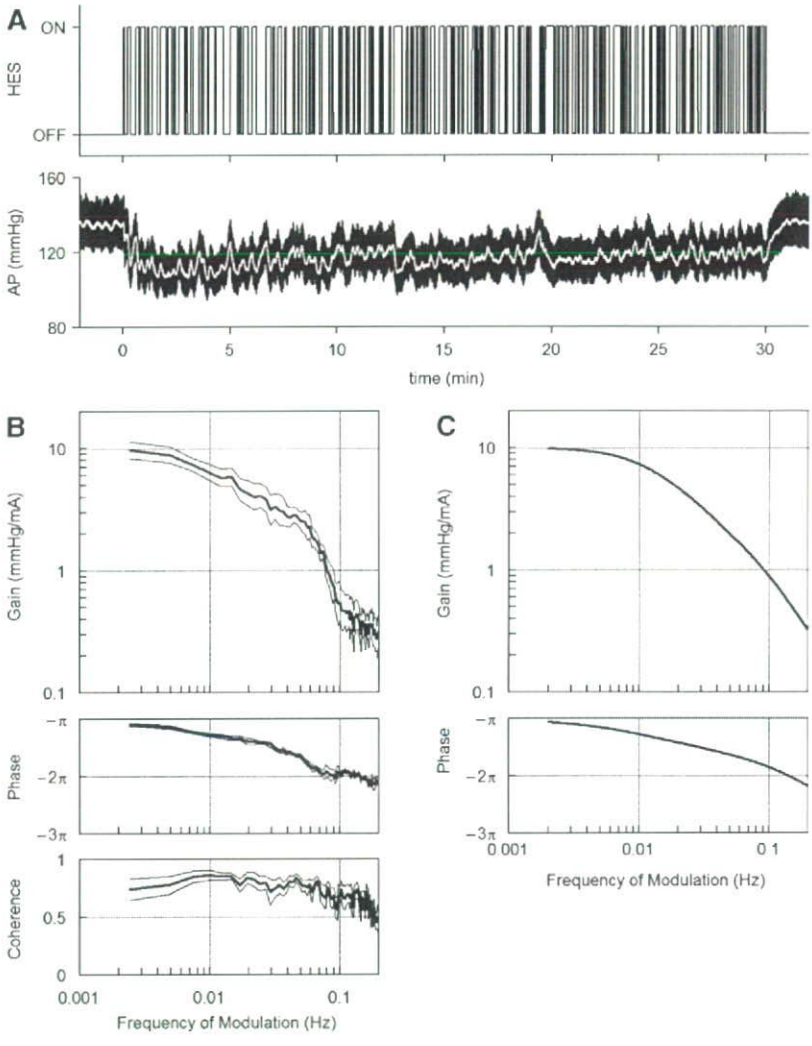

Figure 3. (**A**) Typical recordings of random hind-limb electrical stimulation (HES) and arterial pressure (AP) response. (**B**) Transfer function from HES to the AP response averaged from 8 cats. Thick and thin lines indicate mean and mean±SE values, respectively. (**C**) A model transfer function of the second-order low-pass filter with a lag time that mimics the transfer function from HES to AP.

Results

Relationship Between Stimulus Intensity and AP Response

Typical time series of Protocols 1 and 2 obtained from one animal are shown in **Figures 2A** and **B**, respectively. The pulse width was set in a random order. In Protocol 1, baseline AP obtained at the 0-mA stimulus condition was 118.4±5.4 mmHg across the animals. Changes in mean AP as a function of stimulus current are summarized in **Figure 2C**. The decrease in AP became greater as the stimulus current increased. The overall statistical analysis indicated that the effect of the stimulus current on the magnitude of AP decrease was significant whereas that of pulse width was not. There was no significant interaction effect between the stimulus current and the pulse width.

In Protocol 2, baseline AP at the 0-Hz stimulus condition was 117.6±5.9 mmHg across the animals. Changes in mean AP as a function of stimulus frequency are summarized in **Figure 2D**. The decrease in AP became greater as the stimulus frequency increased from 1 to 10 Hz but it became smaller when the stimulus frequency exceeded 10 Hz. At the pulse width of 1 ms, the stimulus frequency of 100 Hz even increased AP. The overall statistical analysis indicated that the effect of stimulus frequency on the magnitude of AP decrease was significant whereas that of pulse width was not. There was no significant interaction effect between the stimulus frequency and the pulse width.

Dynamic Characteristics of AP Response to HES

Figure 3A depicts a typical time series obtained from Protocol 3. HES was turned on and off randomly, which decreased the mean level of AP and also caused intermittent AP variations. When HES was finally turned off at 30 min, AP began to increase toward the prestimulation value. A long-lasting effect of HES was not observed in the present protocol. The white line in the AP trace represents the 2-s moving averaged data of AP.

The results of transfer function analysis are depicted in **Figure 3B**. In the gain plot, the magnitude of AP response relative to the HES input was plotted in the frequency domain. The gain value became smaller as the frequency increased, indicating the low-pass characteristics of the AP response to HES. In the phase plot, AP showed an out-of-phase relationship with HES at the lowest frequency (0.0024 Hz). The phase delayed more with increasing the frequency of modulation. The coherence value was approximately 0.7 in the frequency range below 0.06 Hz. The

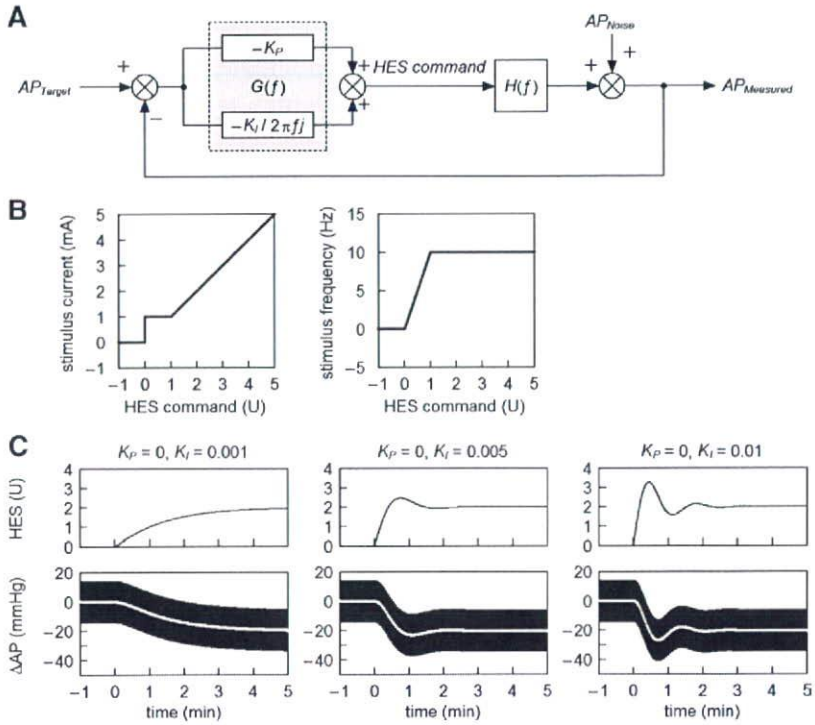

Figure 4. (**A**) A simplified diagram of the feedback controller utilized in the present study. AP_{Target}: target arterial pressure (AP); AP_{Noise}: noise in AP in terms of the control theory; $AP_{Measured}$: measured AP; $G(f)$: transfer function of the controller; $H(f)$: transfer function from hind-limb electrical stimulation (HES) to the AP response; K_P: proportional gain; K_I: integral gain; f and j denote the frequency and imaginary unit, respectively (see Appendix A for details). (**B**) Functions that convert the HES command into the stimulus current and the stimulus frequency. (**C**) Simulation results showing the feedback control of AP by HES. At time zero, the target AP was set at −20 mmHg. In the simulation, a sinusoidal wave (3 Hz, 15 mmHg in amplitude) was added to mimic the pulse pressure in AP. White lines indicate the 2-s moving averaged data of the simulated AP response.

coherence value became smaller in the frequency range above 0.1 Hz but still retained a value of 0.5, indicating that approximately half of the AP variation was explained by the HES input.

The general feature of the dynamic characteristics of the AP response to HES approximated what is known as a second order low-pass filter with a pure dead time, which is mathematically described as:

$$H(f)=\frac{-K}{1+2\zeta\frac{f}{f_N}j+\left(\frac{f}{f_N}j\right)^2}\exp(-2\pi fjL) \quad (3)$$

where K is the steady-state gain, f_N is the natural frequency, ζ is the damping ratio, and L is the pure dead time. When we performed an iterative non-linear least square fitting using a downhill Simplex method, K, f_N, ζ and L were estimated as 10.2±1.6 mmHg/mA, 0.040±0.004 Hz, 1.80±0.24 and 1.38±0.13 s, respectively. A model transfer function shown in **Figure 3C** was drawn using K, f_N, ζ and L of 10 mmHg/mA, 0.04 Hz, 2 and 1 s, respectively.

Development of a Feedback Controller

We used a classical feedback controller to adjust the stimulus intensity of HES[23–25] In reference to **Figure 4A**, a HES command is determined based on a difference between measured and target AP values. $G(f)$ represents the transfer function of the controller with a proportional gain (K_P) and an integral gain (K_I). $H(f)$ indicates the model transfer function shown in **Figure 3C**. A detailed mathematical description of the controller is supplied in Appendix A.

To circumvent a threshold phenomenon in the stimulus current-AP response relationship (see Appendix B for details), the HES command (in an arbitrary unit) was transformed into the stimulus current (in mA) by a factor of 1 (**Figure 4B, Left**) only when the HES command exceeded unity. When the HES command was less than unity, the stimulus current was held at 1 mA and the HES command was transformed into the stimulus frequency (in Hz) by a factor of 10 (**Figure 4B, Right**). The stimulation was turned off when the HES command became negative.

Several sets of simulations were conducted using the model transfer function. The target AP was set at 20 mmHg below the baseline AP. To mimic the pulse pressure in AP, a 3-Hz sinusoidal wave (corresponding to the HR of 180 beats/min) with an amplitude of 15 mmHg (corresponding to the pulse pressure of 30 mmHg) was added to the AP signal. To avoid pulsatile variation in the HES command, we set the proportional gain at zero. Under this condition, when the integral gain was set at 0.001, AP decreased gradually and it took more than 3 min to reach the target AP (**Figure 4C, Left**). When the integral gain was set at 0.005, AP decreased more promptly and reached the target AP in less than 1 min (**Figure 4C, Center**). When the integral gain was set at 0.01, the AP response occurred more rapidly but showed significant oscillations before settling (**Figure 4C, Right**). Based on these simulation results, we set the proportional gain at zero and the integral gain at 0.005 for the actual feedback-control experiment in Protocol 4.

Performance of the Feedback Controller

Figure 5A demonstrates the AP regulation by HES obtained from 2 typical animals. The proportional and integral gains of the controller were not altered among the animals (ie, K_P=0, K_I=0.005). The white line in the AP trace indicates 2-s moving averaged data. The target AP was set at 20 mmHg below the AP value just before the application of HES. The feedback controller was activated for 10 min, which decreased AP at the target level. The HES command was individualized via the feedback mechanism. In the left panel of **Figure 5A**, the HES command gradually increased throughout the 10-min regulation. In the right panel of **Figure 5A**, the HES command was less than unity

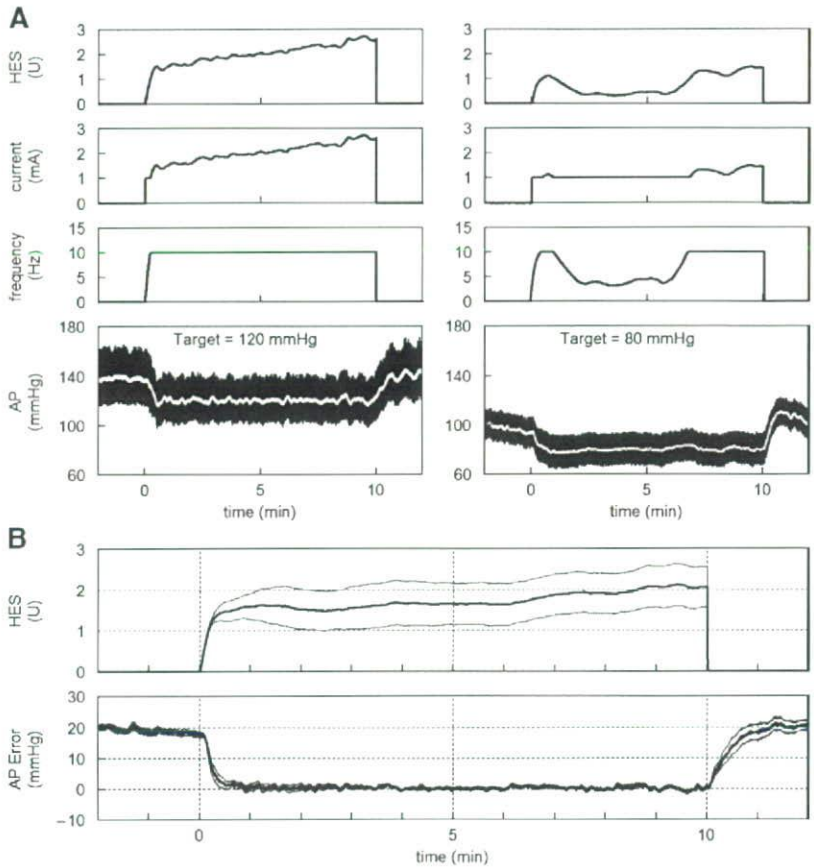

Figure 5. (**A**) Results of 10-min feedback control of arterial pressure (AP) by hind-limb electrical stimulation (HES) obtained from 2 cats. In each cat, the target AP was set at 20 mmHg below the baseline AP value. The current and frequency of HES were automatically adjusted to keep the AP at the target level. (**B**) HES command and the error signal between the target AP and measured AP averaged from 8 cats. The thick and thin lines indicate mean ± SE values, respectively.

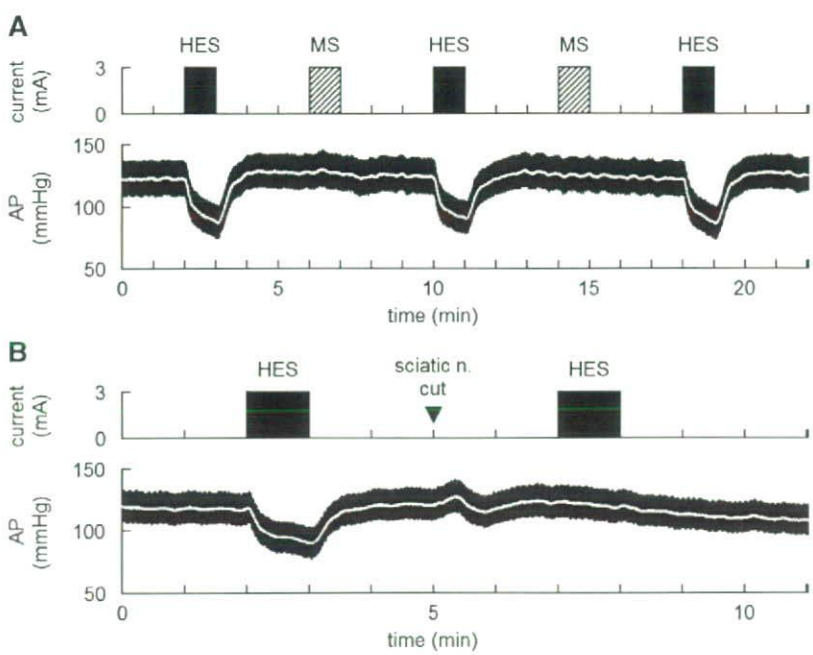

Figure 6. (**A**) Effects of electrical stimulation of the triceps surae muscle (MS) in comparison to hind-limb electrical stimulation (HES). Although muscle twitching was observed, there was no change in arterial pressure (AP) during MS. (**B**) Effects of sectioning the ipsilateral sciatic nerve on the HES-induced changes in AP. After the severance of the ipsilateral sciatic nerve, HES no longer produced significant hypotension.

from 1 to 7 min of the 10-min regulation. In this time period, the HES command altered the stimulus frequency rather than the stimulus current.

Mean and mean ± SE values of the HES command averaged from 8 animals are shown in the top panel of **Figure 5B**. There was a large variance in the HES command among the animals, suggesting inter-individual differences in the responsiveness to HES. The target AP was 102.5±5.6 mmHg across the animals. The error signal between the target AP and measured AP disappeared in less than 1 min (**Figure 5B**,

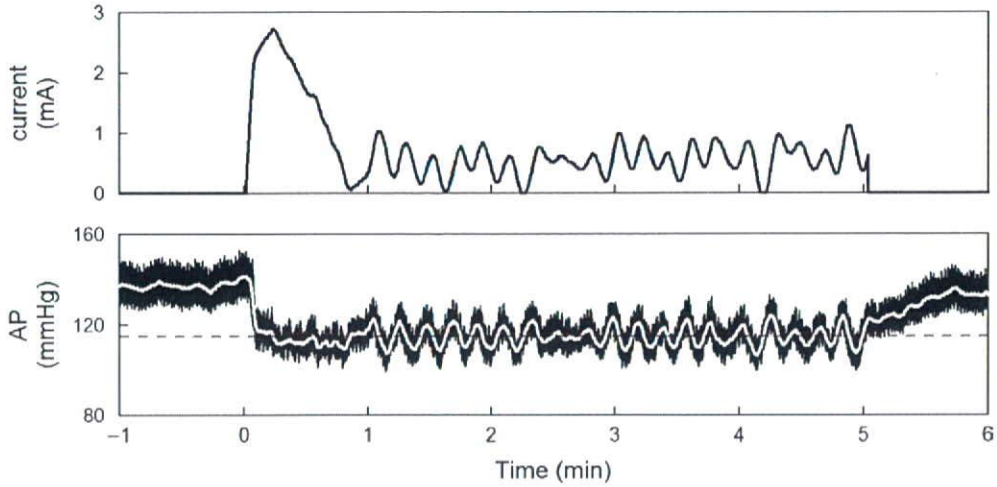

Figure 7. Typical recordings showing failure of controlling the intensity of the hind-limb electrical stimulation during the course of controller development. In this experimental run, only the stimulus current was controlled with a fixed stimulus frequency at 10 Hz. The controller showed on–off type controller behavior once the arterial pressure (AP) approached the target level. The horizontal dashed line indicates the target AP level.

Bottom). The time required for the AP response to reach 90% of the target AP decrease was 38±10 s. Thereafter, the error remained very small until the end of the 10-min regulation. The standard deviation of the steady-state error was 1.3±0.1 mmHg. After the end of the feedback regulation, the error signal gradually returned to approximately 20 mmHg.

Figure 6 represents typical results of the supplemental protocols. Electrical stimulation of the triceps surae muscle (denoted as "MS") did not change AP significantly in spite of visible twitching of the stimulated muscle, suggesting that the depressor response to HES was not the outcome of the direct muscle stimulation (**Figure 6A**). Sectioning the ipsilateral sciatic nerve abolished the depressor effect of HES, suggesting that somatic afferent signals were delivered through the sciatic nerve to the central nervous system during HES (**Figure 6B**).

Discussion

We identified the dynamic input–output relationship between HES and the AP response. By using the model transfer function from HES to AP, we were able to develop a servo-controller that automatically adjusted the HES command to reduce AP at a prescribed target level.

Development of the Feedback Controller

The stimulus current-AP response relationship showed a monotonous decreasing slope (**Figure 2C**). Because the effect of the pulse width was statistically insignificant, we chose the stimulus current as a primary control variable. The problem with using the stimulus current for the control variable was that a certain threshold current existed between 0 and 1 mA where the AP response to HES became discontinuous. If the stimulus current happened to be feedback controlled near the threshold current, AP showed significant oscillation around the target level (**Figure 7**, see Appendix B for details). To avoid such a problem related to the threshold current, we set the minimum current to 1 mA (above the threshold current) and used the stimulus frequency as a secondary control variable (**Figure 4B**).

The stimulus frequency-AP response relationship revealed a valley-shaped curve with the nadir of approximately 10 Hz (**Figure 2D**). The result is similar to that obtained by stimulating hamstring muscle afferent nerves?[6] From the viewpoint of controller design, the valley-shaped input–output relationship is troublesome because the proportional-integral controller only assumes a monotonous input–output relationship?[3] To avoid the problem of the valley-shaped input–output relationship, we limited the stimulus frequency to the range from 0 to 10 Hz (**Figure 4B, Right**). A similar strategy of selecting the monotonous input–output portion was used in a previous study![12]

We quantified the dynamic AP response to HES using a transfer function analysis (**Figure 3B**), and modeled it by a second-order low-pass filter with a pure dead time (**Figure 3C**). Once the transfer function is modeled, we could construct a numerical simulator for the feedback controller design (**Figure 4A**). Because the optimization of control parameters usually requires a number of trials, even if the initial values are selected via classical methods such as the Ziegler–Nichols' method?[3] it is impractical to determine optimal parameter values without using the simulator. The simulation results indicated that the integral gain value of 0.005 would provide rapid and stable AP regulation (**Figure 4C**). Because the controller was designed via intensive simulations, AP was actually controlled at the target level with a small variance (**Figure 5B, Bottom**). Note that the current and frequency of HES were automatically adjusted and individualized via the feedback mechanism (**Figure 5A**).

Bionic Strategies Using Neural Interfaces

A framework of treating cardiovascular diseases using neural interfaces is intriguing because the autonomic nervous system exerts powerful influences on the circulatory system. In previous studies, we identified the dynamic characteristics of the arterial baroreflex system and used them to design an artificial vasomotor center. The artificial vasomotor center was able to control AP by stimulating the celiac ganglia in anesthetized rats[10,11] or the spinal cord in anesthetized cats![12] The strength and rapidity of the neural effect on the cardiovascular system compared with that of the

humoral effect[27,28] make the neural interventions desirable for the rapid and stable restoration of AP against acute disturbances such as those induced by postural changes. Gotoh et al demonstrated that a direct neural interface to the rostral ventrolateral medulla also enabled rapid and stable restoration of AP during nitroprusside-induced hypotension in conscious rats.[29] The bionic system to control AP has also been applied in human subjects.[13]

Although the aforementioned bionic systems aimed to maintain AP against acute hypotension by increasing sympathetic nerve activity,[10–13,29] sympathoinhibition might also be required for the treatment of cardiovascular diseases accompanying sympathetic overactivity. Baroreceptor activation is one of the potential sympathoinhibitory neural modulation.[8,9] In the present study we only demonstrated a framework of short-term AP control by HES. With a development of proper implanting electrodes, however, we might be able to control AP chronically using HES. Although carotid sinus baroreceptor stimulation has a potential to treat drug-resistant hypertension,[9] it could activate peripheral chemoreflex by stimulating carotid bodies. HES might circumvent such unintentional chemoreflex activation. Another clinical implication will be the treatment of chronic heart failure. Although the vagal effect of HES was not evaluated in the present study, acupuncture stimulation might facilitate cardiac vagal activity.[30] Because chronic intermittent vagal nerve stimulation increased the survival of chronic heart failure rats,[7] chronic intermittent HES might be used as an alternative method of direct vagal nerve stimulation for the treatment of chronic heart failure.

Study Limitations

First, we did not identify the mechanism of HES. Because sectioning of the ipsilateral sciatic nerve abolished the AP response to HES (**Figure 6B**), somatic afferent is involved in the effect of HES. In a series of studies, Chao et al and Li et al demonstrated that electroacupuncture activated group III and IV fibers in the median nerves and inhibited sympathetic outflow via activation of μ- and δ-opioid receptors in the rostral ventrolateral medulla.[31,32] Whether a similar mechanism underlies in the rapid-onset and short-lasting effect of HES awaits further studies.

Second, we used pentobarbital anesthesia. Although peripheral neurotransmissions of norepinephrine and acetylcholine can be assessed under the same anesthesia,[28,33] because pentobarbital can suppress many neurotransmitters in the central nervous system,[34] anesthesia might compromise the HES effect. Further studies are required to establish the utility of HES in awake conditions.

Third, we set the proportional gain of the controller at zero to avoid pulsatile changes in the HES command. However, other approaches such as that using a low-passed signal of measured AP as a controlled variable might also be effective to avoid the pulsatile variation in the HES command.

Finally, a development of implanting electrodes is the prerequisite for chronic use of HES. Intramuscular electrodes used in functional electrical stimulation might be used for HES but further refinements are clearly needed regarding the positioning of electrodes including the depth of implantation.[35,36]

In conclusion, we identified the dynamic characteristics of the AP response to acupuncture-like HES and demonstrated that a servo-controlled HES system was able to reduce AP at a prescribed target level. Although further studies are required to identify the mechanism of HES to reduce AP, acupuncture-like HES would be an additional modality to exert a quantitative depressor effect on the cardiovascular system.

Acknowledgments

This study was supported by the following Grants: "Health and Labour Sciences Research Grant for Research on Advanced Medical Technology", "Health and Labour Sciences Research Grant for Research on Medical Devices for Analyzing, Supporting and Substituting the Function of Human Body", "Health and Labour Sciences Research Grant (H18-Iryo-Ippan-023) (H18-Nano-Ippan-003) (H19-Nano-Ippan-009)", from the Ministry of Health, Labour and Welfare of Japan, and the "Industrial Technology Research Grant Program" from New Energy and Industrial Technology Development Organization of Japan.

References

1. Bilgutay AM, Bilgutay IM, Merkel FK, Lillehei CW. Vagal tuning: A new concept in the treatment of supraventricular arrhythmias, angina pectoris, and heart failure. *J Thorac Cardiovasc Surg* 1968; **56:** 71–82.
2. Braunwald E, Epstein SE, Glick G, Wechsler AS, Braunwald NS. Relief of angina pectoris by electrical stimulation of the carotid-sinus nerves. *N Engl J Med* 1967; **277:** 1278–1283.
3. Schwartz SI, Griffith LS, Neistadt A, Hagfors N. Chronic carotid sinus nerve stimulation in the treatment of essential hypertension. *Am J Surg* 1967; **114:** 5–15.
4. Vanoli E, De Ferrari GM, Stramba-Badiale M, Hull SS Jr, Foreman RD, Schwartz PJ. Vagal stimulation and prevention of sudden death in conscious dogs with a healed myocardial infarction. *Circ Res* 1991; **68:** 1471–1481.
5. Yang JL, Chen GY, Kuo CD. Comparison of effect of 5 recumbent positions on autonomic nervous modulation in patients with coronary artery disease. *Circ J* 2008; **72:** 902–908.
6. Baba R, Koketsu M, Nagashima M, Inasaka H, Yoshinaga M, Yokota M. Adolescent obesity adversely affects blood pressure and resting heart rate. *Circ J* 2007; **71:** 722–726.
7. Li M, Zheng C, Sato T, Kawada T, Sugimachi M, Sunagawa K. Vagal nerve stimulation markedly improves long-term survival after chronic heart failure in rats. *Circulation* 2004; **109:** 120–124.
8. Zucker IH, Hackley JF, Cornish KG, Hiser BA, Anderson NR, Kieval R, et al. Chronic baroreceptor activation enhances survival in dogs with pacing-induced heart failure. *Hypertension* 2007; **50:** 904–910.
9. Mohaupt MG, Schmidli J, Luft FC. Management of uncontrollable hypertension with a carotid sinus stimulation device. *Hypertension* 2007; **50:** 825–828.
10. Sato T, Kawada T, Shishido T, Sugimachi M, Alexander J Jr, Sunagawa K. Novel therapeutic strategy against central baroreflex failure: A bionic baroreflex system. *Circulation* 1999; **100:** 299–304.
11. Sato T, Kawada T, Sugimachi M, Sunagawa K. Bionic technology revitalizes native baroreflex function in rats with baroreflex failure. *Circulation* 2002; **106:** 730–734.
12. Yanagiya Y, Sato T, Kawada T, Inagaki M, Tatewaki T, Zheng C, et al. Bionic epidural stimulation restores arterial pressure regulation during orthostasis. *J Appl Physiol* 2004; **97:** 984–990.
13. Yamasaki F, Ushida T, Yokoyama T, Ando M, Yamashita K, Sato T. Artificial baroreflex: Clinical application of a bionic baroreflex system. *Circulation* 2006; **113:** 634–639.
14. Li P, Pitsillides KF, Rendig SV, Pan HL, Longhurst JC. Reversal of reflex-induced myocardial ischemia by median nerve stimulation: A feline model of electroacupuncture. *Circulation* 1998; **97:** 1186–1194.
15. Longhurst JC. Electroacupuncture treatment of arrhythmias in myocardial ischemia. *Am J Physiol Heart Circ Physiol* 2007; **292:** H2032–H2034.
16. Lujan HL, Kramer VJ, DiCarlo SE. Electroacupuncture decreases the susceptibility to ventricular tachycardia in conscious rats by reducing cardiac metabolic demand. *Am J Physiol Heart Circ Physiol* 2007; **292:** H2550–H2555.
17. Ohsawa H, Okada K, Nishijo K, Sato Y. Neural mechanism of depressor responses of arterial pressure elicited by acupuncture-like stimulation to a hindlimb in anesthetized rats. *J Auton Nerv Syst* 1995; **51:** 27–35.
18. Uchida S, Shimura M, Ohsawa H, Suzuki A. Neural mechanism of bradycardiac responses elicited by acupuncture-like stimulation to a hind limb in anesthetized rats. *J Physiol Sci* 2007; **57:** 377–382.
19. Michikami D, Kamiya A, Kawada T, Inagaki M, Shishido T, Yamamoto K, et al. Short-term electroacupuncture at Zusanli resets the arterial baroreflex neural arc toward lower sympathetic nerve

activity. *Am J Physiol Heart Circ Physiol* 2006; **291:** H318–H326.
20. Yamamoto H, Kawada T, Kamiya A, Kita T, Sugimachi M. Electroacupuncture changes the relationship between cardiac and renal sympathetic nerve activities in anesthetized cats. *Auton Neurosci: Basic and Clinical* 2008; **144:** 43–49.
21. Marmarelis PZ, Marmarelis VZ. Analysis of Physiological Systems. The white noise method in system identification. New York: Plenum; 1978.
22. Snedecor GW, Cochran WG. Statistical Methods, 8th ed. Ames, Iowa: University Press; 1989.
23. Åström K, Hägglund T. PID Controllers: Theory, Design, and Tuning, 2nd ed. City of Publication: Instrument Society of America; 1995.
24. Kawada T, Sunagawa G, Takaki H, Shishido T, Miyano H, Miyashita H, et al. Development of a servo-controller of heart rate using a treadmill. *Jpn Circ J* 1999; **63:** 945–950.
25. Kawada T, Ikeda Y, Takaki H, Sugimachi M, Kawaguchi O, Shishido T, et al. Development of a servo-controller of heart rate using a cycle ergometer. *Heart Vessels* 1999; **14:** 177–184.
26. Johansson B. Circulatory responses to stimulation of somatic afferents with special reference to depressor effects from muscle nerves. *Acta Physiol Scand* 1962; **Suppl 198:** 1–91.
27. Kawada T, Miyamoto T, Miyoshi Y, Yamaguchi S, Tanabe Y, Kamiya A, et al. Sympathetic neural regulation of heart rate is robust against high plasma catecholamines. *J Physiol Sci* 2006; **56:** 235–245.
28. Kawada T, Yamazaki T, Akiyama T, Shishido T, Miyano H, Sato T, et al. Interstitial norepinephrine level by cardiac microdialysis correlates with ventricular contractility. *Am J Physiol Heart Circ Physiol* 1997; **273:** H1107–H1112.
29. Gotoh TM, Tanaka K, Morita H. Controlling arterial blood pressure using a computer-brain interface. *Neuroreport* 2005; **16:** 343–347.
30. Nishijo K, Mori H, Yosikawa K, Yazawa K. Decreased heart rate by acupuncture stimulation in humans via facilitation of cardiac vagal activity and suppression of cardiac sympathetic nerve. *Neurosci Lett* 1997; **227:** 165–168.
31. Chao DM, Shen LL, Tjen-A-Looi S, Pitsillides KF, Li P, Longhurst JC. Naloxone reverses inhibitory effect of electroacupuncture on sympathetic cardiovascular reflex responses. *Am J Physiol Heart Circ Physiol* 1999; **276:** H2127–H2134.
32. Li P, Tjen-A-Looi SC, Longhurst JC. Rostral ventrolateral medullary opioid receptor subtypes in the inhibitory effect of electroacupuncture on reflex autonomic response in cats. *Auton Neurosci: Basic and Clinical* 2001; **89:** 38–47.
33. Kawada T, Yamazaki T, Akiyama T, Li M, Ariumi H, Mori H, et al. Vagal stimulation suppresses ischemia-induced myocardial interstitial norepinephrine release. *Life Sci* 2006; **78:** 882–887.
34. Adachi YU, Yamada S, Satomoto M, Watanabe K, Higuchi H, Kazama T, et al. Pentobarbital inhibits L-DOPA-induced dopamine increases in the rat striatum: An in vivo microdialysis study. *Brain Res Bull* 2006; **69:** 593–596.
35. Guevremont L, Norton JA, Mushahwar VK. Physiologically based controller for generating overground locomotion using functional electrical stimulation. *J Neurophysiol* 2007; **97:** 2499–2510.
36. Hardin E, Kobetic R, Murray L, Corado-Ahmed M, Pinault G, Sakai J, et al. Walking after incomplete spinal cord injury using an implanted FES system: A case report. *J Rehabil Res Dev* 2007; **44:** 333–346.

Appendix A

Framework of the Feedback Controller

Figure 4A is a simplified block diagram of the feedback controller system used in the present study. The controller was based on a proportional-integral controller[23–25] $G(f)$ represents the transfer function of the controller.

$$G(f)=-K_P+\frac{-K_I}{2\pi fj} \quad \text{(A1)}$$

where K_P and K_I denote proportional and integral gains, respectively. j represents the imaginary unit. Negative signs for the proportional and integral gains compensate for the negative input–output relationship between HES and the AP response. $H(f)$ represents a model transfer function from HES to AP determined from Protocol 3. The measured AP can be expressed as:

$$AP_{Measured}(f)=H(f)HES(f)+AP_{Noise}(f) \quad \text{(A2)}$$

where $AP_{Noise}(f)$ is the AP fluctuation such as that associated with changes in animal conditions. The controller compares the measured AP with the target AP, and adjusts the HES command to minimize the difference between them according to the following equation:

$$HES(f)=G(f)[AP_{Target}(f)-AP_{Measured}(f)] \quad \text{(A3)}$$

By eliminating $HES(f)$ from the equations A2 and A3, the overall controller characteristics are described as:

$$AP_{Measured}(f)=\frac{G(f)H(f)}{1+G(f)H(f)}AP_{Target}(f)+\frac{1}{1+G(f)H(f)}AP_{Noise}(f) \quad \text{(A4)}$$

The equation A4 indicates that if $G(f)$ is properly selected so that $G(f)H(f)$ becomes by far greater than unity, the measured AP approaches the target AP whereas the noise term is significantly attenuated over the frequency range of interest.

Appendix B

Problem with the Threshold Current

We tried to adjust the intensity of HES by the stimulus current alone. When the stimulus current happened to be feedback controlled near a threshold current, however, the controller showed an on–off type controller behavior around the target AP level, as shown in **Figure 7**. At time zero, the controller was activated. The stimulus current increased to approximately 2.7 mA in the beginning and then decreased to a value below 1 mA, accompanying the AP reduction around a target level (a horizontal dashed line). However, the stimulus current and AP did not stabilize. Because the AP response was discontinuous at the threshold current (ie, the depressor effect of HES was abruptly turned on and off), the controller could not adjust the stimulus current in a continuous manner. To avoid this kind of on–off type controller behavior, we introduced the stimulus frequency as the secondary control variable (**Figure 4B**).

Inhibition of Tumor Necrosis Factor-α–Induced Interleukin-6 Expression by Telmisartan Through Cross-Talk of Peroxisome Proliferator-Activated Receptor-γ With Nuclear Factor κB and CCAAT/Enhancer-Binding Protein-β

Qingping Tian, Ryohei Miyazaki, Toshihiro Ichiki, Ikuyo Imayama, Keita Inanaga, Hideki Ohtsubo, Kotaro Yano, Kotaro Takeda, Kenji Sunagawa

Abstract—Telmisartan, an angiotensin II type 1 receptor antagonist, was reported to be a partial agonist of peroxisome proliferator-activated receptor-γ. Although peroxisome proliferator-activated receptor-γ activators have been shown to have an anti-inflammatory effect, such as inhibition of cytokine production, it has not been determined whether telmisartan has such effects. We examined whether telmisartan inhibits expression of interleukin-6 (IL-6), a proinflammatory cytokine, in vascular smooth muscle cells. Telmisartan, but not valsartan, attenuated IL-6 mRNA expression induced by tumor necrosis factor-α (TNF-α). Telmisartan decreased TNF-α–induced IL-6 mRNA and protein expression in a dose-dependent manner. Because suppression of IL-6 mRNA expression was prevented by pretreatment with GW9662, a specific peroxisome proliferator-activated receptor-γ antagonist, peroxisome proliferator-activated receptor-γ may be involved in the process. Telmisartan suppressed IL-6 gene promoter activity induced by TNF-α. Deletion analysis suggested that the DNA segment between −150 bp and −27 bp of the IL-6 gene promoter that contains nuclear factor κB and CCAAT/enhancer-binding protein-β sites was responsible for telmisartan suppression. Telmisartan attenuated TNF-α–induced nuclear factor κB– and CCAAT/enhancer-binding protein-β–dependent gene transcription and DNA binding. Telmisartan also attenuated serum IL-6 level in TNF-α–infused mice and IL-6 production from rat aorta stimulated with TNF-α ex vivo. These data suggest that telmisartan may attenuate inflammatory process induced by TNF-α in addition to the blockade of angiotensin II type 1 receptor. Because both TNF-α and angiotensin II play important roles in atherogenesis through enhancement of vascular inflammation, telmisartan may be beneficial for treatment of not only hypertension but also vascular inflammatory change. (***Hypertension*. 2009;53: 798-804.**)

Key Words: interleukin-6 ■ TNF-α ■ PPARγ ■ NF-κB ■ C/EBPβ

Angiotensin II (Ang II) is a main final effecter molecule of the renin–angiotensin system. Physiologically, Ang II plays an important role in the regulation of blood pressure, fluid volume, and electrolyte balance.[1] However, Ang II is also involved in the pathological processes, such as cardiovascular diseases, renal insufficiency, and metabolic disorders.[2] Indeed, inhibition of the renin–angiotensin system by Ang II type 1 receptor (AT1R) antagonists has been proven beneficial for treatment of heart failure,[3] chronic kidney diseases,[4] and myocardial infarction.[5] AT1R antagonists also showed favorable effects on prevention of new onset of diabetes mellitus and atrial fibrillation.[6,7]

Telmisartan, one of the AT1R antagonists, was reported to be a partial agonist of peroxisome proliferator-activated receptor-γ (PPARγ).[8,9] PPARγ is a nuclear receptor transcription factor,[10] and the target genes of PPARγ are involved in the regulation of lipid and glucose metabolism and adipocyte differentiation. In addition, it is reported that thiazolidinediones (TZDs), synthetic PPARγ ligands, have an anti-inflammatory effect and inhibit atherogenesis.[11] The anti-inflammatory effect of TZDs involves inhibition of the function of nuclear factor κB (NF-κB), which plays an important role in the expression of many genes mediating an inflammatory process.[12]

Interleukin-6 (IL-6) is one of the proinflammatory cytokines and is induced by tumor necrosis factor-α (TNF-α),[13] Ang II,[14] and other stimuli in vascular smooth muscle cells (VSMCs), endothelial cells, and macrophages. IL-6 plays an

Received November 17, 2008; first decision November 24, 2008; revision accepted February 23, 2009.

From the Departments of Cardiovascular Medicine (Q.T., R.M., T.I., I.I., K.I., H.O., K.Y., K.T., K.S.) and Advanced Therapeutics for Cardiovascular Diseases (T.I., K.T.), Kyushu University Graduate School of Medical Sciences, and Peking University First Hospital (Q.T.), Fukuoka, Japan.

Q.T., R.M., and I.I. contributed equally to this work.

Correspondence to Toshihiro Ichiki, MD, PhD, Department of Cardiovascular Medicine, Kyushu University Graduate School of Medical Sciences, 3-1-1 Maidashi, Higashi-ku, 812-8582 Fukuoka, Japan. E-mail ichiki@cardiol.med.kyushu-u.ac.jp

Hypertension **is available at http://hyper.ahajournals.org** **DOI: 10.1161/HYPERTENSIONAHA.108.126656**

important role in vascular remodeling and was reported to be a useful biomarker in predicting future cardiovascular events.[15]

Telmisartan has been shown to induce differentiation of adipocytes through activation of PPARγ. A recent study showed that telmisartan attenuated hepatic steatosis, inflammation, and fibrosis in a rat model of nonalcoholic steatohepatitis.[16] It was also reported that telmisartan treatment of patients with hypertension and coronary heart disease decreased β2-integrin MAC-1 expression in peripheral lymphocytes independent of Ang II.[17] These data suggest that telmisartan has an anti-inflammatory effect independently of AT1R blocking effect. However, an anti-inflammatory effect of telmisartan on blood vessel is incompletely characterized. Therefore, we tested whether telmisartan inhibits TNF-α–induced IL-6 expression through PPARγ in VSMCs.

Materials and Methods

DMEM was purchased from GIBCO/BRL. FBS was from JRH Biosciences. Recombinant TNF-α was a generous gift from Dainippon-Sumitomo Pharmaceutical Co (Osaka, Japan). Telmisartan was a generous gift from Boehringer Ingelheim (Ingelheim, Germany). Valsartan was purchased from US Pharmacopeia. BSA and GW9662 were purchased from Sigma. Pioglitazone was purchased from LKT Laboratories. [α-^{32}P] dCTP and [γ-^{32}P]ATP were purchased from Perkin-Elmer Life Sciences. Antibodies against extracellular signal-regulated protein kinase (ERK), p38 mitogen-activated protein kinase (MAPK), c-Jun N-terminal kinase (JNK), and their phosphorylated forms were purchased from Cell Signaling Technology. Other reagents were purchased from Wako Pure Chemicals unless otherwise mentioned specifically. TNF-α was dissolved in DMEM with 0.1% BSA, and Ang II was suspended in sterile water. Other reagents that added to culture medium were dissolved in dimethyl sulfoxide at a final concentration of 0.1%, which did not show any effect on IL-6 induction.

Cell Culture

VSMCs were isolated from the thoracic aorta of Sprague–Dawley rats and cultured in a humidified atmosphere of 95% air/5% CO_2 at 37°C in DMEM as described previously.[14] Cells were grown to confluence and growth-arrested in DMEM with 0.1% BSA for 2 days before use. Passages between 5 and 13 were used for the experiments.

Northern Blotting

Total RNA was prepared according to the acid guanidinium thiocyanate-phenol-chloroform extraction method. Northern blot analysis of IL-6 mRNA and 18S ribosomal RNA (rRNA) was performed as described previously.[14] The radioactivity of hybridized bands of IL-6 mRNA and rRNA was quantified with a MacBAS Bioimage Analyzer (Fuji Photo Film). It was reported that 2 species of IL-6 mRNA were generated by an alternative polyadenylation.[18] The intensity of both bands was taken into account for quantification.

Quantification of Rat IL-6 by Sandwich ELISA

VSMCs were stimulated with TNF-α (10 ng/mL) or Ang II (100 nmol/L) for 24 hours in the presence or absence of telmisartan (1 to 20 μmol/L). Then the medium of VSMCs was collected and centrifuged at 12 000 rpm for 1 minute. The supernatant was stored at −70°C until used for the assay. ELISA for rat IL-6 was performed with a Cytoscreen ELISA kit (BioSource International) according to manufacturer instructions. The measurement was performed in duplicate.

Transfection of IL-6 Promoter–Luciferase Fusion DNA Construct to VSMCs

The IL-6 gene promoter–luciferase fusion DNA constructs and luciferase assay were described previously.[14] Detailed protocols can be found in an online data supplement available at http://hyper.ahajournals.org.

Plasmids of NF-κB–luciferase and CCAAT/enhancer-binding protein-β (C/EBPβ)–luciferase were purchased from Stratagene Co. Five copies of NF-κB consensus sequence or 3 copies of C/EBPβ consensus sequence were ligated to minimal promoter followed by luciferase gene.

Gel Mobility Shift Assay

Gel mobility shift assay was performed as described previously[14] using synthetic NF-κB and C/EBPβ DNA probe (NF-κB: CAT GTG GGA TTT TCC CAT GA; C/EBPβ: CAC ATT GCA CAA TCT TAA). Detailed protocols are indicated in the online supplement.

Effect of Telmisartan on Ang II– and TNF-α–Induced IL-6 Production In Vivo

All procedures were approved by the institutional animal use and care committee and were conducted in conformity with institutional guidelines of Kyushu University. Ang II (490 ng/kg per minute) or TNF-α (80 ng/kg per minute) was administered subcutaneously to 9-week-old C57/BL6 mice (Kyudo Co; Saga, Japan) by osmotic mini-pump (Alzet) for 1 week. Doses of TNF-α and Ang II were determined in a preliminary experiment to detect a significant increase in the serum IL-6 level. Telmisartan was dissolved in water (10 μg/mL) and administered ad libitum. The estimated dose of orally ingested telmisartan was 2 mg/kg per day. Blood pressure and heart rate were measured using tail-cuff method (UR-5000; UEDA). After 1 week, mice were euthanized under pentobarbital anesthesia, and peripheral blood was collected from inferior vena cava. The serum concentration of IL-6 was measured using ELISA kit (R&D Systems). No significant differences in body weight were observed among the treatment groups (data not shown).

Ex Vivo Stimulation of Rat Aorta

Nine-week-old Sprague-Dawley rats were purchased from Kyudo Co. Rats were euthanized under deep pentobarbital anesthesia. The aorta was excised and adventitia was removed. The aorta was cut into 6 pieces and stimulated with TNF-α (50 ng/mL) or Ang II (1 μmol/L) in the absence or presence of telmisartan (10 μmol/L) in 500 μL of DMEM supplemented with 0.1% BSA for 48 hours. Concentrations of Ang II and TNF-α were determined in a preliminary experiment to detect a significant increase in the production of IL-6 in the supernatant of ex vivo–cultured aortic segments. The supernatant was subjected to ELISA to measure IL-6 production. The IL-6 concentration in the supernatant was normalized with the wet weight of the aortic segment.

RT-PCR and Western Blot Analysis

Detailed protocols are indicated in the online supplement.

Statistical Analysis

Statistical analysis was performed with 1-way ANOVA and Fisher's test if appropriate. A P value <0.05 was considered statistically significant. Values are expressed as mean±SEM.

Results

Telmisartan Attenuated TNF-α–Induced IL-6 Expression

VSMCs were incubated with or without telmisartan (10 μmol/L) for 60 minutes. Then the cells were stimulated with TNF-α (10 ng/mL) for 30 minutes. Northern blot analysis revealed attenuation of TNF-α–induced IL-6 mRNA expression by telmisartan (Figure 1A). However, valsartan (10 μmol/L), another AT1R antagonist, failed to suppress TNF-α–induced IL-6 mRNA expression (Figure 1B). Telmisartan (1 to 20 μmol/L) dose-dependently suppressed TNF-α–induced IL-6 mRNA expression (Figure 1C). The concentration range of telmisartan was chosen based on a previous

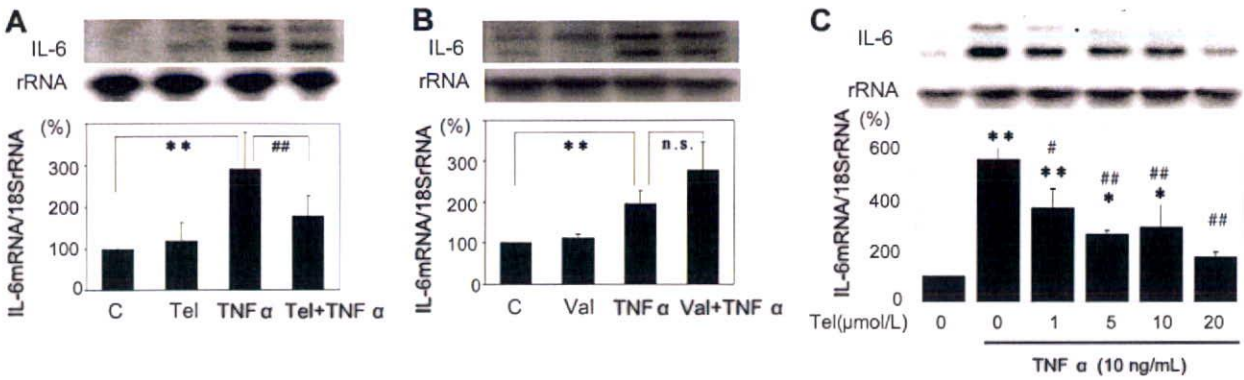

Figure 1. Suppression of TNF-α–induced IL-6 mRNA expression by telmisartan (Tel). VSMCs were preincubated with Tel (10 μmol/L; A), valsartan (Val; 10 μmol/L; B), or various concentrations (1 to 20 μmol/L; C) of telmisartan for 60 minutes and stimulated with TNF-α (10 ng/mL) for 30 minutes. Total RNA was isolated, and expression of IL-6 mRNA and 18S rRNA was determined by Northern blot analysis. Radioactivity of IL-6 mRNA was measured with an imaging analyzer and was normalized by radioactivity of rRNA. Values (mean±SEM) are expressed as percentage of control culture in a bar graph (100%; No. of independent experiments was 5). *P<0.05; **P<0.01 vs control; #P<0.05; ##P<0.01 vs TNF-α.

clinical study[19] that showed that the steady-state serum level of telmisartan was 1 to 5 μmol/L when 80 to 160 mg per day of telmisartan was given for 7 days to patients with essential hypertension. And it was reported that telmisartan at concentrations >25 μmol/L stimulated PPARα.[9] Therefore, we did not use telmisartan at concentrations >20 μmol/L in this study.

The protein level of IL-6 in the supernatant of VSMCs was measured after 24 hours of stimulation with TNF-α (10 ng/mL) with or without preincubation with telmisartan (1 to 20 μmol/L). TNF-α–induced IL-6 protein expression was also dose-dependently attenuated by telmisartan (Figure 2A). Ang II (100 nmol/L)–induced IL-6 production was inhibited completely by telmisartan at lower concentrations (Figure 2B); thus, we confirmed that telmisartan is an effective AT1R antagonist.

We next examined whether telmisartan affected TNF receptor expression. Semiquantitative RT-PCR analysis showed that telmisartan did not affect TNF type 1 receptor mRNA expression (supplemental Figure IB). We could not detect TNF type 2 receptor mRNA in our VSMCs. We also examined the effect of telmisartan on TNF-α–induced MAPK activation (supplemental Figure II). Telmisartan did not affect TNF-α–induced activation of ERK, p38MAPK, or JNK.

Telmisartan Inhibition of TNF-α–Induced IL-6 Expression Was Dependent on PPARγ

To clarify the role of PPARγ in telmisartan inhibition of TNF-α–induced IL-6 expression, the effect of GW9662, a PPARγ-specific antagonist, was examined. Although GW9662 itself did not affect IL-6 mRNA expression, preincubation with GW9662 (10 μmol/L; 3 hours) blocked telmisartan inhibition of TNF-α–induced IL-6 expression (Figure 3A). Pioglitazone (10 μmol/L; preincubation for 1 hour), a full PPARγ agonist, also suppressed the TNF-α–induced IL-6 mRNA expression (Figure 3B).

Telmisartan-Inhibited IL-6 Gene Promoter Activity

Next, the effect of telmisartan on IL-6 gene promoter activity was examined. TNF-α (10 ng/mL) increased IL-6 gene promoter activity by 2-fold. Preincubation with telmisartan (10 μmol/L) significantly inhibited IL-6 gene promoter activity (Figure 4). Deletion analysis of the IL-6 gene promoter suggested that the DNA segment between −150 bp and −27 bp was responsible for the downregulation by telmisartan (Figure 4A) because telmisartan inhibited the luciferase activity in the −150-bp construct, but the −27-bp

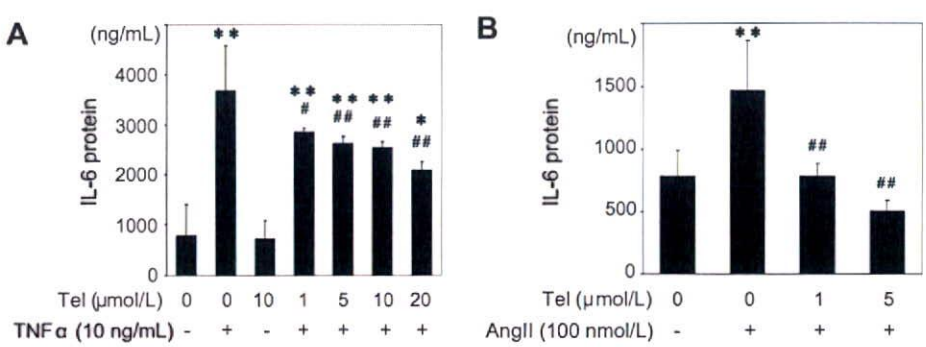

Figure 2. Suppression of TNF-α– and Ang II–induced IL-6 protein production by telmisartan (Tel). A, VSMCs were preincubated with Tel (10 μmol/L) at various concentrations for 60 minutes and stimulated with TNF-α (10 ng/mL) for 24 hours. B, VSMCs were incubated with Tel at 1 or 5 μmol/L and stimulated with Ang II (100 nmol/L) for 24 hours. IL-6 protein production in the supernatant of VSMCs was measured by ELISA. *P<0.05 vs control; **P<0.01 vs control; #P<0.05 vs TNF-α; ##P<0.01 vs TNF-α or Ang II (No. of independent experiment was 6 in duplicate).

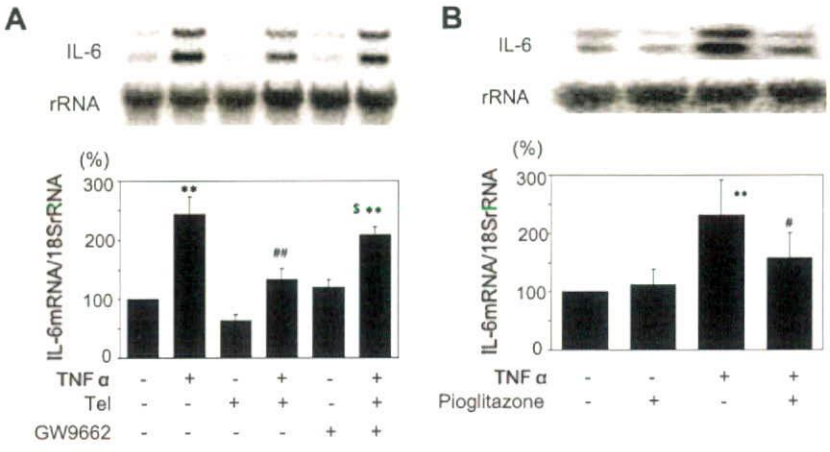

Figure 3. Effect of GW9662 on telmisartan (Tel) inhibition of TNF-α–induced IL-6 expression. A, VSMCs were incubated with GW9662 (10 μmol/L) for 3 hours followed by preincubation with Tel (10 μmol/L) for 60 minutes. Then the VSMCs were stimulated with TNF-α (10 ng/mL) for 30 minutes. B, VSMCs were preincubated with pioglitazone (10 μmol/L) for 60 minutes, then stimulated with TNF-α (10 ng/mL) for 30 minutes. Northern blot analysis of IL-6 mRNA was performed as described in Figure 1 legend. **$P<0.01$ vs control; #$P<0.05$ vs TNF-α; ## $P<0.01$ vs TNF-α; \$$P<0.05$ vs Tel+TNF-α (No. of independent experiments was 4).

construct no longer responded to TNF-α or telmisartan. The DNA segment between −150 bp and −27 bp contains NF-κB and C/EBPβ as consensus cis DNA elements.[20] We therefore examined whether telmisartan inhibited NF-κB– and C/EBPβ-dependent gene transcription activated by TNF-α. As shown in Figure 4B, telmisartan inhibited TNF-α–induced activation of luciferase activity, which is solely dependent on NF-κB or C/EBPβ.

The gel mobility shift assay showed that telmisartan inhibited TNF-α–induced NF-κB DNA binding activity (Figure 5A). Telmisartan also attenuated TNF-α–induced C/EBPβ DNA binding activity to a lesser extent (Figure 5B).

Telmisartan Attenuated IL-6 Production In Vivo and Ex Vivo

To confirm that telmisartan inhibits IL-6 production in vivo, Ang II (490 ng/kg per minute) or TNF-α (80 ng/kg per minute) was administered to mice with or without telmisartan (2 mg/kg per day) for 1 week. Ang II but not TNF-α increased blood pressure level (Table). Ang II–induced high blood pressure was inhibited by telmisartan. Heart rate was not significantly different among the treatment groups. Ang II–induced increase in serum IL-6 level was almost completely inhibited by telmisartan, and telmisartan significantly attenuated TNF-α–induced IL-6 production (Figure 6A). To

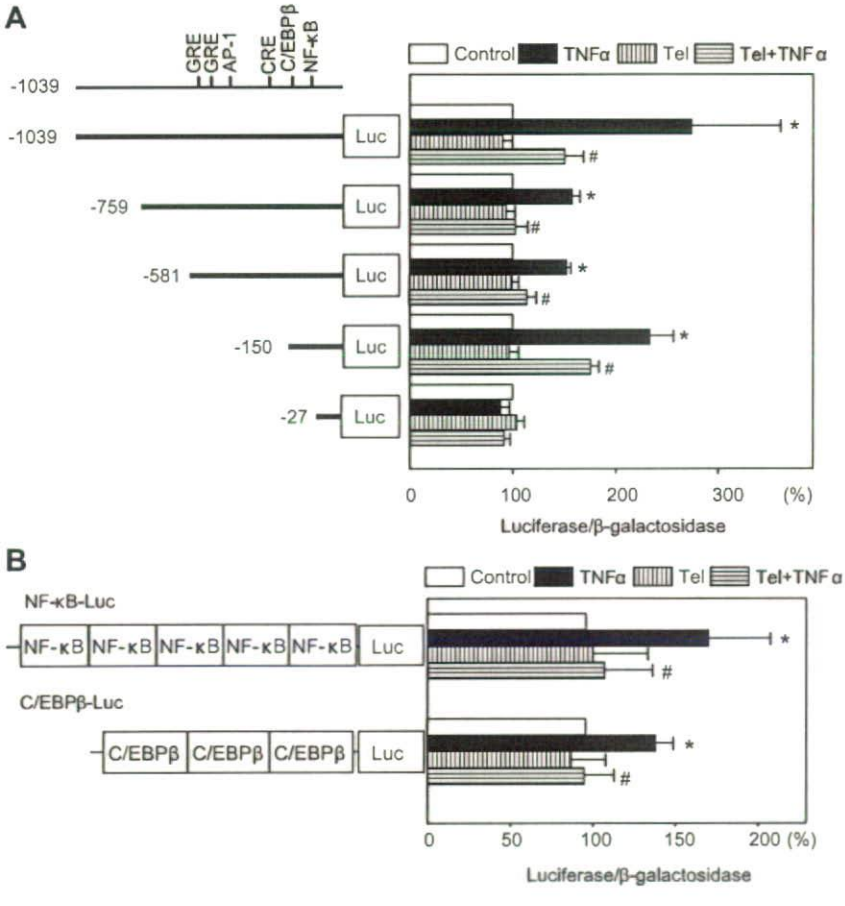

Figure 4. Suppression of IL-6 gene promoter activity by telmisartan (Tel). A, After transfection of IL-6 gene promoter/luciferase (Luc) fusion DNA (5 μg), VSMCs were preincubated with or without Tel (10 μmol/L; 60 minutes) and stimulated with TNF-α (10 ng/mL) for 24 hours. AP-1 indicates activator protein-1. B, NF-κB–Luc or C/EBPβ–Luc was introduced to VSMCs. VSMCs were preincubated with or without Tel (10 μmol/L; 60 minutes) and stimulated with TNF-α (10 ng/mL) for 24 hours. Luc activity was normalized with β-galactosidase activity. The relative promoter activity without stimulation (control) was set as 100%. *$P<0.01$ vs control; #$P<0.05$ vs TNF-α (No. of independent experiments was 4).

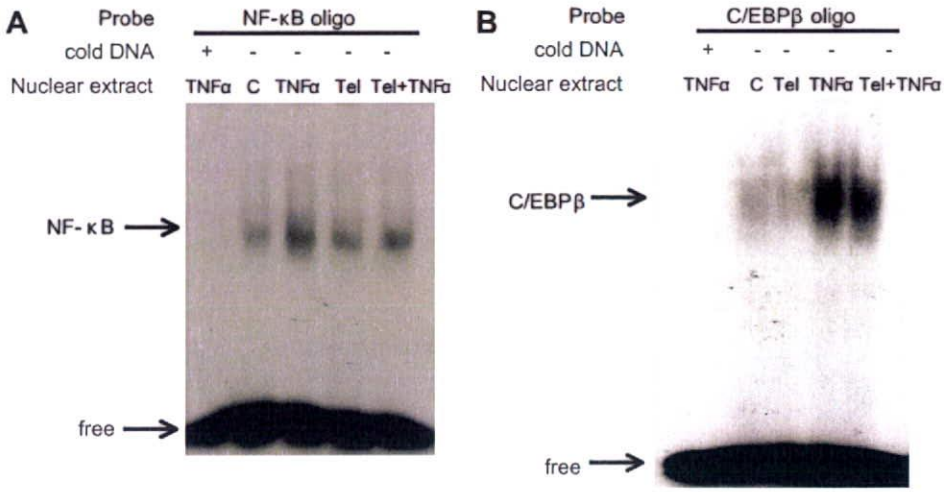

Figure 5. Telmisartan (Tel) attenuated TNF-α–induced NF-κB and C/EBPβ binding. A, Binding activity of NF-κB sequence of IL-6 gene promoter to nuclear extracts from unstimulated (C), TNF-α–stimulated, Tel-stimulated, and Tel- and TNF-α–stimulated VSMCs were examined by gel mobility shift assay. B, Binding activity of C/EBPβ sequence of IL-6 gene promoter to nuclear extracts from unstimulated, Tel-stimulated, TNF-α–stimulated, and Tel- and TNF-α–stimulated VSMCs were examined by gel mobility shift assay. Fifty times molar excess of unlabeled oligonucleotide (oligo) was added to the reaction mixture in the left lane (Cold DNA+). The same results were obtained in other independent experiments (No. of independent experiment was 3).

confirm that IL-6 is produced from blood vessel, a segment of rat aorta without adventitia was stimulated ex vivo with Ang II (1 μmol/L) or TNF-α (50 ng/mL) in the presence or absence of telmisartan (10 μmol/L) for 48 hours. Production of IL-6 induced by TNF-α in the supernatant was significantly attenuated by coincubation with telmisartan (Figure 6B). Ang II–induced production of IL-6 was completely inhibited by telmisartan. These results were consistent with those obtained during in vitro experiments.

Discussion

In the present study, we demonstrated that telmisartan but not valsartan suppressed TNF-α–induced IL-6 expression through a PPARγ-dependent manner. Inhibition of NF-κB and C/EBPβ DNA binding activity by telmisartan may be responsible for attenuation of TNF-α–induced IL-6 expression. This is the first study demonstrating that telmisartan modulates cytokine production induced by non–Ang II stimulus. The in vivo and ex vivo results were consistent with those obtained from the in vitro study. The in vivo study showed that telmisartan had an anti-inflammatory effect in mice, and the ex vivo study indicated that IL-6 was produced from blood vessel in response to TNF-α stimulation, and telmisartan attenuated the induction.

On activation by ligands, PPARγ regulates expression of several genes involved in lipid and carbohydrate metabolism and inflammatory responses.[21] PPARγ regulates gene expression through 2 different transcriptional regulatory mechanisms: transactivation and transrepression. Transactivation depends on PPARγ response element. On activation, PPARγ forms a heterodimer with retinoid X receptor and binds to PPARγ response element in the promoter region of the target genes.[22] In contrast, transrepression involves an interference with other transcription factors such as NF-κB and activator protein 1.[22] Although telmisartan was reported to be a partial agonist of PPARγ, it has not been determined whether telmisartan regulates gene expression through transrepression mechanism. Our data suggest that telmisartan may have a transrepression effect on gene expression in addition to AT1R blockade.

The mechanism of transrepression by PPARγ activators is less well known. A recent study showed that PPARγ activation by TZD induced sumoylation of PPAR, resulting in retention of nuclear receptor corepressor/histone deacetylase complex to the promoter and suppression of gene transcription.[12] Troglitazone, another TZD, inhibited TNF-α–induced and NF-κB–dependent gene transcription without affecting NF-κB nuclear translocation or DNA binding in adipocytes,[23] which may support the above-mentioned model. However, a previous study showed that TZDs inhibited IL-1β–activated NF-κB and C/EBPβ DNA binding to the IL-6 gene promoter.[24] It was also reported that troglitazone inhibited TNF-α–induced IL-6 expression in multiple myeloma cells by inhibiting NF-κB and C/EBPβ DNA binding.[25] In this study, activated PPARγ competed for PPARγ coactivator-1, a transcription coactivator, with NF-κB, resulting in attenua-

Table. Heart Rate and Blood Pressure of Ang II– and TNF-α–Treated Mice

Variable	Control	Tel	Ang II	Tel+Ang II	TNF-α	Tel+TNF-α
HR (bpm)	576±24	598±21	599±18	608±27	611±47	586±22
BP (mm Hg)	95.3±1.3	94.0±2.8	109.6±4.7*	102.2±1.8†	97.3±0.9	95.5±1.4

HR indicates heart rate; BP, blood pressure.
*$P<0.05$ vs control; †$P<0.05$ vs Ang II; n=5.